Earthquake mechanisms of the Adriatic Sea and Western Greece: implications for the oceanic subduction-continental collision transition

Calum Baker, Denis T Hatzfeld, Hélène Lyon-Caen, Elephteria Papadirnitriou, Alexis Rigo

▶ **To cite this version:**

Calum Baker, Denis T Hatzfeld, Hélène Lyon-Caen, Elephteria Papadirnitriou, Alexis Rigo. Earthquake mechanisms of the Adriatic Sea and Western Greece: implications for the oceanic subduction-continental collision transition. Geophysical Journal International, 1997, 131 (3), pp.559 - 594. 10.1111/j.1365-246X.1997.tb06600.x . hal-01415818

HAL Id: hal-01415818
https://hal.science/hal-01415818

Submitted on 13 Dec 2016

HAL is a multi-disciplinary open access archive for the deposit and dissemination of scientific research documents, whether they are published or not. The documents may come from teaching and research institutions in France or abroad, or from public or private research centers.

L'archive ouverte pluridisciplinaire **HAL**, est destinée au dépôt et à la diffusion de documents scientifiques de niveau recherche, publiés ou non, émanant des établissements d'enseignement et de recherche français ou étrangers, des laboratoires publics ou privés.

Geophys. J. Int. (1997) **131**, 559–594

Earthquake mechanisms of the Adriatic Sea and Western Greece: implications for the oceanic subduction–continental collision transition

Calum Baker,[1,*] Denis Hatzfeld,[1] Hélène Lyon-Caen,[2] Elephteria Papadimitriou[3] and Alexis Rigo[2,†]

[1] *Laboratoire de Géophysique Interne et Tectonophysique, IRIGM,* BP53, 38041 *Grenoble Cedex 9, France. E-mail: hatzfeld@lgit.observ-gr.fr*
[2] *Institut de Physique du Globe,* 4 *place Jussieu,* CP 89, 75252 *Paris Cedex* 05, *France*
[3] *Geophysical Laboratory, Aristotelian University,* PO Box 352–1, 540–06 *Thessaloniki, Greece*

Accepted 1997 June 23. Received 1997 June 23; in original form 1996 November 20

SUMMARY

We present 21 focal solutions (magnitude >5.5) reliably computed by body-wave modelling for the western Hellenic arc from Yugoslavia to the southern Peloponnese. Mechanisms located within the Aegean show normal faulting, the T-axis trending N–S in the centre and parallel to the active boundary in the external part. Mechanisms associated with the Keffalinia fault are consistent with dextral strike-slip motion. Reverse mechanisms located along the active boundary are remarkably consistent and do not depend on the nature of the active boundary (continental collision or oceanic subduction). The consistency in azimuth of the slip vectors and of the GPS velocity relative to Africa, all along the active boundary, suggests that the deformation is related to the same motion. The discrepancy between seismic-energy release and the amount of shortening confirms that the continental collision is achieved by seismic slip on faults but the oceanic subduction is partially aseismic. The northward decrease in velocity between continental collision and oceanic subduction suggests the continental collision to be a recent evolution of the active subduction.

Key words: Adriatic Sea, continental collision, earthquake mechanisms, oceanic subduction, Western Greece.

1 INTRODUCTION

The Aegean region is one of the most rapidly deforming and seismically active continental regions, which makes it important for the study of continental tectonics (Jackson 1994). Focal mechanisms of strong earthquakes provide some information on this deformation. McKenzie (1972, 1978), Anderson & Jackson (1987) and Papazachos, Kiratzi & Papadimitriou (1991), among others, have published focal mechanisms computed from first-motion polarities for the Aegean, and the inferred geodynamics leads to models which are not without controversy (e.g. McKenzie 1978; Le Pichon & Angelier 1979). The accuracy of some of the mechanisms was, however, sometimes questionable. The waveform-modelling inversion technique (Nábelek 1984) allows better constraint of the fault-plane-solution parameters. In addition, the source function, the depth and the seismic moment of the event are obtained. Several recent studies have used this waveform-inversion technique to determine well-constrained source parameters in the Aegean for different areas (e.g. Taymaz, Jackson & Westaway 1990; Taymaz, Jackson & McKenzie 1991; Papadimitriou 1993) or for individual earthquakes (e.g. Kiratzi & Langston 1989, 1991; Lyon-Caen *et al.* 1988). These studies have concentrated on the central part of Greece, the Aegean Sea and the Hellenic Trench subduction zone, and have greatly added to our understanding of the geometry of deformation and kinematic processes in these areas.

In this paper we use waveform modelling to study the large earthquakes in Western Greece and the Adriatic Sea. This very active region is of particular interest for several reasons: it is located at the transition between the active subduction zone that occurs beneath the Hellenic arc and the continental collision between Apulia and continental Greece. It is also located near the pole of rotation that Le Pichon & Angelier (1979) and Le Pichon *et al.* (1995) proposed for the Hellenic trench. Here we present 21 new solutions and discuss the source parameters for 32 large (magnitude >5.5) earthquakes

* Now at: Department of Earth Sciences, University of Keele, Staffordshire, UK.
† Now at: OMP-GRGS, CNRS-UMR5562, 14 av. E. Belin, 31400 Toulouse, France.

© 1997 RAS

Downloaded from http://gji.oxfordjournals.org/ at Observatoire de la CÃ'te d'Azur - Geoazur on December 13, 2016

which have occurred in Western Greece and the Adriatic between 1959 and 1988.

2 GEODYNAMIC SETTING

The Aegean is a region of intense deformation located between two major lithospheric plates, the European plate and the African plate (Fig. 1), whose relative convergent motion is N–S and of about 1 cm yr^{-1} (Argus *et al.* 1989). However, the relative motion across the Hellenic trench as inferred by seismology (e.g. McKenzie 1978; Jackson 1994) or geodesy (e.g. Noomen *et al.* 1994) is NE–SW and greater than 5 cm yr^{-1} and is related to the lithospheric subduction of Africa beneath the Aegean. The difference in the relative motion is likely to be due to the motion of the Turkish plate along the North Anatolian fault and to the important amount of internal deformation that occurs within the Aegean.

The seismicity along the coast of the former Yugoslavia, Albania and NW Greece defines the eastern boundary of the 'Adriatic Block' as a promontory of the African Plate. While it is generally agreed (e.g. Channell, D'Argenio & Horvath 1979) that the structural complexity of the Adriatic orogenic belts indicates that this region was part of the African plate during Jurassic and Cretaceous times, geophysical as well as tectonic evidence suggests that this is no longer the case. Anderson & Jackson (1987) showed that the motions along the boundaries of the Adriatic Block derived from earthquake slip-vector directions are significantly different from those shown by events associated with African–Eurasian plate convergence. This is consistent with VLBI (Ward 1994) and SLR (Noomen *et al.* 1994) geodetic observations.

To the north, the convergence between Apulia and the Hellenides, the Albanides and the Dinarides is a continental-type collision. To the south, the lithosphere of the Ionian basin is probably oceanic and the convergent motion results in subduction beneath the Hellenic trench. The transition between the active lithospheric subduction and the continental collision is located around the Ionian islands (McKenzie 1978; Anderson & Jackson 1987), where the Kefallinia strike-slip transform zone is located (Cushing 1985; Scordilis *et al.* 1985; Kahle *et al.* 1993). This termination is marked by a sharp bathymetric slope, striking at N20°. This dextral strike-slip transform zone was assumed to be the northern limit of the mobile Akarnania block. However, palaeomagnetic results show that the clockwise rotation in northern, as in southern, Albania has remained the same as in the Ionian islands and in the Peloponnese since the late Eocene (Speranza *et al.* 1995).

Tectonic observations (Sorel 1989; Waters 1993) as well as focal mechanisms of microearthquakes (Hatzfeld *et al.* 1995) show predominant N–S extension in a more internal domain within Epirus and Akarnania. The Gulf of Corinth (Rigo *et al.* 1996) and Macedonia (Soufleris & Stewart 1981) also exhibit N–S extension. The transition between extension and compression in the western Hellenides is not well located.

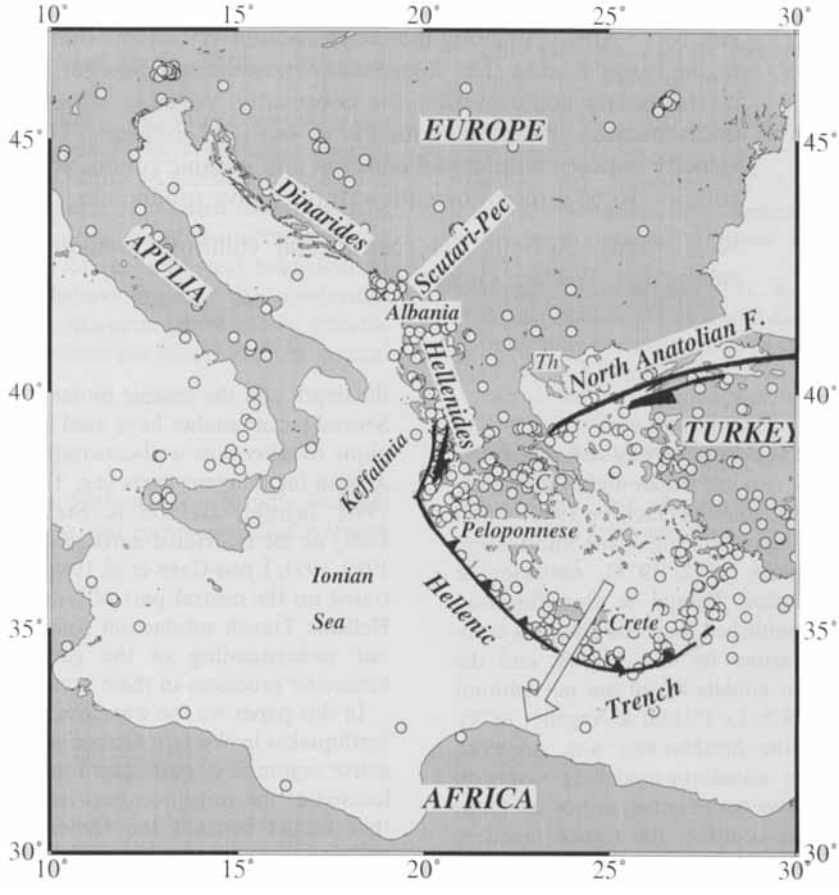

Figure 1. General sketch of the area showing the main features and geographical names. The North Anatolian fault transfers the motion of Turkey towards the southwest. The Hellenic trench and the Scutari–Pec fault are indicated. Earthquakes of magnitude greater than 5 (NEIC file) are displayed. The white arrow is the direction of motion of Aegea relative to Europe deduced from SLR measurement (Noomen *et al.* 1994).

Downloaded from http://gji.oxfordjournals.org/ at Observatoire de la CÃ'te d'Azur - Geoazur on December 13, 2016

We shall investigate the focal mechanisms of strong earthquakes in this zone in greater detail in this paper.

3 DATA REDUCTION AND MODELLING

We use the algorithm developed by McCaffrey, Abers & Zwick (1991) to calculate the source parameters for all earthquakes of magnitude >5.5. It is based on Nabelek's (1984) inversion procedure, which minimizes, in a least-squares sense, the misfit between observed and synthetic seismograms. The procedure has been used in a number of recent studies of seismicity and only a brief overview of the method is presented here. The reader is referred to McCaffrey & Nabelek (1987) for details.

We use the *P* and *SH* waveforms that are recorded on long-period instruments from the WWSSN and GDSN. To avoid the effect of upper-mantle structure and interference from core phases, only stations in the range $30°<\Delta<90°$ for *P* waves and $30°<\Delta<75°$ for *SH* waves are used. Data from the WWSSN network were obtained by digitizing paper enlargements of microfiche records. The seismograms were digitized at uneven sampling intervals, care being taken to include the peaks, troughs and inflection points in the data. The waveform was then interpolated using a weighted average-slope method to provide the evenly sampled curve required in the inversion. The WWSSN seismograms were corrected to take into account the non-orthogonality of the time and amplitude scales and to scale the data to a common instrument amplification. The appropriate instrument type may be obtained from the WWSSN record together with any clock correction which must be accounted for in order to ensure accurate timing of the phase arrivals. In one case (the event of 1959 November 15) the earthquake occurred before the installation of the WWSSN. In this case we assumed the magnification of the instruments to be the same as later, but the inferred moment is therefore only indicative. For the data obtained from the GDSN network, the instrument response is taken into account by considering the poles and zeros of the system frequency response.

The data window for each seismogram starts immediately before the onset of the direct phase (*P* or *S*) and includes the near-source reflected and converted phases (*pP*, *sP* and *sS*). The waveforms from the north and east components are rotated to obtain the transverse *SH* waveform. The arrival times for the direct phases are read, whenever possible, from the corresponding short-period record. When a short-period record is not available, the theoretical phase arrival is calculated using the ISC epicentre and origin time and the Jeffreys–Bullen traveltime tables.

For each station, the inversion procedure adjusts the relative amplitudes of the source time function elements, the centroid depth, the seismic moment and the fault parameters (strike, dip, rake) to minimize, in a weighted-least-square sense, the misfit between observed and synthetic seismograms. We refer to this solution as the 'minimum-misfit solution'. The seismograms are normalized to a common instrument magnification and epicentral distance, and are weighted in the inversion to minimize the bias in the azimuthal distribution of the data (Nabelek 1984). It has been shown that the covariance matrix associated with this solution usually underestimates the true uncertainties associated with the source parameters (McCaffrey & Nabelek 1987). Here we use the method adopted by several authors (e.g. McCaffrey & Nabelek 1987; Nelson *et al.* 1987; Frederich, McCaffrey & Denham 1988; Molnar & Lyon-Caen 1989) where the source parameters are fixed at values close to, but different from, those of the minimum-misfit solution. We then estimate whether the match of the observed to the synthetic seismograms deteriorates significantly. This is considered to give a better estimate of the true uncertainties. An example of this approach is given in Fig. A4 for event 4 (1965 July 6), which is discussed in Section 3.3.

The largest uncertainties in the seismic moment and centroid depth arise from errors in the source velocity model, and the trade-off between the source function and the depth. While we do not have accurate crustal-velocity structures for the region around the Adriatic and Ionian seas, we have chosen values which we consider to be realistic based on the average velocities derived in a study by Panagiotopoulos & Papazachos (1985). We have taken the crustal velocity structure to consist of a layer over a half-space. The upper layer has a *P*-wave velocity of 6.0 km s^{-1}, an *S*-wave velocity of 3.7 km s^{-1} and a density of 2.75 g cm^{-3}, and the lower half-space has a *P*-wave velocity of 6.8 km s^{-1}, an *S*-wave velocity of 3.9 km s^{-1} and a density of 2.9 g cm^{-3}. A water layer above the upper layer is included for events located beneath the sea. This velocity structure may certainly be considered as a simplification. In particular, we have not included a Moho. This is because the modelling algorithm used allows us to include at most a layer over a half-space and the earthquake focus is constrained to lie below the upper layer. The main effect of this is that only reverberations within the upper-crustal layer and water layer (where present) are taken into account in the modelling procedure. Specifically, no reverberations between the Moho and the free surface or the Moho and other crustal layers are considered. Studies (e.g. Nabelek 1984) have shown that the amplitudes of these reverberations are not generally large compared to the effect of other factors such as source depth, source time function and source multiplicity. However, the inability of the modelling to match secondary arrivals at some stations for some events may be explained in part by the simplified crustal structure used. In particular, near-source heterogeneities may explain why the seismograms for stations at one azimuth appear considerably more complex than those in other parts of the focal sphere for some events.

A minimum-misfit solution is the only result of an inversion given by the computer algorithm and therefore may not represent the true solution if the data are contaminated by noise, or if the procedure converges towards a secondary minimum. For some events, we computed an *a priori* solution, taking into account other information that we believe is relevant (such as surface ruptures during the earthquake, local tectonics, bathymetry, etc.). In most cases, this consists of fixing the strike of the fault plane to be consistent with local tectonics. This is especially justified for shallow-dipping planes which are not well constrained by the modelling, but whose azimuth is known. Our final choice between this *a priori* (or preferred) solution and the minimum-misfit solution is made by comparing the fit of the seismograms at certain key stations to ensure that it did not deteriorate significantly.

The source parameters of the 21 events in this study are presented in Table 1(a), and shown in Fig. 2. The double-couple mechanisms are specified in terms of strike, dip and rake, following the convention of Aki & Richards (1980). We

Downloaded from http://gji.oxfordjournals.org/ at Observatoire de la CÃ'te d'Azur - Geoazur on December 13, 2016

Table 1. (a) Parameters of the fault-plane solutions, this study. (b) Parameters of the fault-plane solutions, previous studies.

No	Date y–m–d	Origin h:m:s	Location Lat N (°)	Lon E (°)	mb	Ms	Mo $\times 10^{16}$ Nm	Centr. depth km	Strike 1 (°) N	Dip 1 (°)	Rake 1 (°)	Strike 2 (°) N	Dip 2 (°)	Rake 2 (°)	Slip (°) N	R
(a)																
1	59–11–15	17:08:40	37.83	20.56	6.6		1630	13±5	134±03	7±10	−90±20	313	83	−90	223	
2	63–12–16	13:47:56	37.10	20.90	5.6		19	6±5	291±20	7±10	74±30	127	83	92	217	
3	64–04–13	08:29:60	45.27	18.04	5.4		40	11±4	282±30	52±06	79±20	120	39	104	210	
4	65–07–06	03:18:42	38.37	22.40	5.8		167	10±4	281±25	34±10	−71±15	79	58	−102	169	
5	66–02–05	02:01:45	39.10	21.74	5.6		246	11±4	263±30	40±25	−95±20	90	50	−86	180	
6	66–10–29	02:39:25	38.90	21.10	5.7		23	15±4	324±30	40±15	48±30	194	62	119	284	
7	67–05–01	07:09:03	39.60	21.29	5.6		99	10±6	153±30	42±15	−85±25	335	48	−95	245	
8	67–11–30	07:23:50	41.41	20.44	5.9		220	9±5	190±30	43±10	−88±15	7	47	−91	97	
9	69–07–08	08:09:13	37.50	20.31	5.4	5.4	73	10±5	346±25	13±20	108±25	147	78	86	237	
10	72–09–17	14:07:16	38.28	20.34	5.6	6.3	27	8±4	39±15	61±08	−173±30	306	84	−29	216	
11	73–11–04	15:52:12	38.89	20.44	5.8	5.5	61	23±7	324±40	50±10	81±25	158	41	100	248	
12	76–05–11	16:59:48	37.56	20.35	5.8	6.4	56	13±4	323±15	13±10	90±30	143	77	90	233	
13	78–05–23	23:34:11	40.73	23.25	5.6	5.8	62	8±4	265±25	40±20	−82±30	76	50	−96	166	
14	79–04–15	06:19:44	42.09	19.21	6.2	6.9	2483	12±6	316±30	14±20	90±30	136	76	90	226	
15	79–04–15	14:43:06	42.32	18.68	5.7	5.6	41	8±4	339±25	10±12	113±35	135	81	86	225	
16	79–05–24	17:23:18	42.26	18.75	5.8	6.2	102	6±4	322±20	35±10	90±25	142	55	90	232	
17	80–05–18	20:02:57	43.29	20.84	5.7	5.8	60	10±5	200±06	79±08	167±10	292	78	11	202	
18	82–11–16	23:41:21	40.88	19.59	5.6	5.5	17	17±4	323±30	27±10	92±25	141	63	89	231	
19	83–01–17	12:41:31	38.03	20.23	6.1	7.0	208	11±5	48±20	56±05	167±25	145	80	35	235	
20	83–03–23	23:51:07	38.29	20.26	5.8	6.2	29	7±5	30±25	70±10	176±25	121	86	20	211	
21	86–09–13	17:24:31	37.01	22.18	6.0	6.1	65	8±4	196±25	51±20	−90±20	16	39	−90	106	
(b)																
1*	65–03–31	09:46:26	38.38	22.26	6.3		1704	55	136	76	78	357	18	130	46	1
2*	70–04–08	13:50:28	38.34	22.56	5.8		91	9	265	23	−81	75	67	266	345	1
3*	72–09–13	04:13:20	37.96	22.38	5.8		163	80	133	65	164	229	76	26	140	1
4*	78–06–20	20:03:21	40.78	23.24	6.1	6.4	424	7	271	42	−74	70	50	−104	340	1
5*	81–02–24	20:53:37	38.10	22.84	6.1	6.7	875	12±2	264±15	42±5	−80±10	71	49	−99	340	2
6*	81–02–25	02:35:53	38.14	23.05	5.7	6.4	397	8±2	241±06	44±5	−85±10	54	46	−95	324	2
7*	81–03–04	21:58:07	38.18	23.17	5.8	6.2	270	7±3	230±05	45±5	−90±10	50	45	−90	320	2
8*	85–04–30	18:14:13	39.26	22.81	5.4	5.5	30	11±2	77±05	50±5	−105±05	280	42	−73	190	2
9*	92–11–18	21:10:41	38.30	22.45	5.8	5.7	41	7.4±1	270±07	30±3	−81±07	100	60	95	350	3
10*	95–05–13	08:47:13	40.18	21.66	6.2	6.6	620	11±1	240±01	40±05	−85±05	53	50	−94	323	4
11*	95–06–15	00:15:49	38.36	22.20	6.1	6.2	340	7.2±1	277±01	33±05	−76±05	80	58	−99	170	5

Plan1 is assumed to be the fault plane. Strike, Dip and Rake follow Aki & Richards (1980) convention. Slip is the azimuth of the slip vector relative to the North.
R is the reference: 1 Liotier (1989); 2 Taymaz *et al.* (1991); 3 Hatzfeld *et al.* (1996a); 4 Hatzfeld *et al.* (1996b); 5 Bernard *et al.* (1997).

present both planes and assume Plane 1 to be the active fault plane, taking into consideration other information such as surface faulting and aftershock patterns. The minimum-misfit solution, together with the observed (solid) and synthetic (dashed) waveforms are shown in a series of diagrams (Figs A1–A21). The upper part of each diagram shows the *P* waveforms and the lower part the *SH* waveforms. The nodal planes of the direct *P* and nodal surfaces of the *SH* waves are shown on lower-hemisphere, equal-area projections. The source time function, formed from a series of overlapping triangles, is shown in the centre of each figure. For every event we show the minimum-misfit solution, and we conduct tests to compare it with other solutions or to check its stability. In some cases, our preferred solution is different from the minimum-misfit solution because the poor station coverage allows a range of acceptable solutions. Below, we discuss the main features of each earthquake. For convenience, we have divided the area of study into three regions: the Adriatic, where continental collision is occurring, the Ionian Sea, where a strike-slip zone is present, and Central Greece, where extension is observed.

3.1 Adriatic Sea zone

1964 April 13, event 3, Fig. A3

This earthquake occurred in the northern part of the former Yugoslavia. The minimum-misfit solution is constrained by a reasonable coverage of *P* waveforms, but only a small number of *SH* waveforms were large enough to be used. The solution shows almost pure thrust faulting on a fault plane striking approximately N100°. This solution is close to that obtained by Anderson & Jackson (1987), but different from McKenzie's (1972) model. No surface break for this or other events in the area has been reported (Anderson & Jackson 1987) and it is not possible to say whether the north- or south-dipping nodal plane is the fault plane.

We conducted tests to compare this solution to other possibilities. A pure dip-slip mechanism (line 2, Fig. A3b) shows a slightly worse fit for the *SH* wave at BLA. The solution similar to the one proposed by McKenzie (1972) shows a worse fit in the *SH* waveform, especially for CHG

Downloaded from http://gji.oxfordjournals.org/ at Observatoire de la CÃ´te d'Azur - Geoazur on December 13, 2016

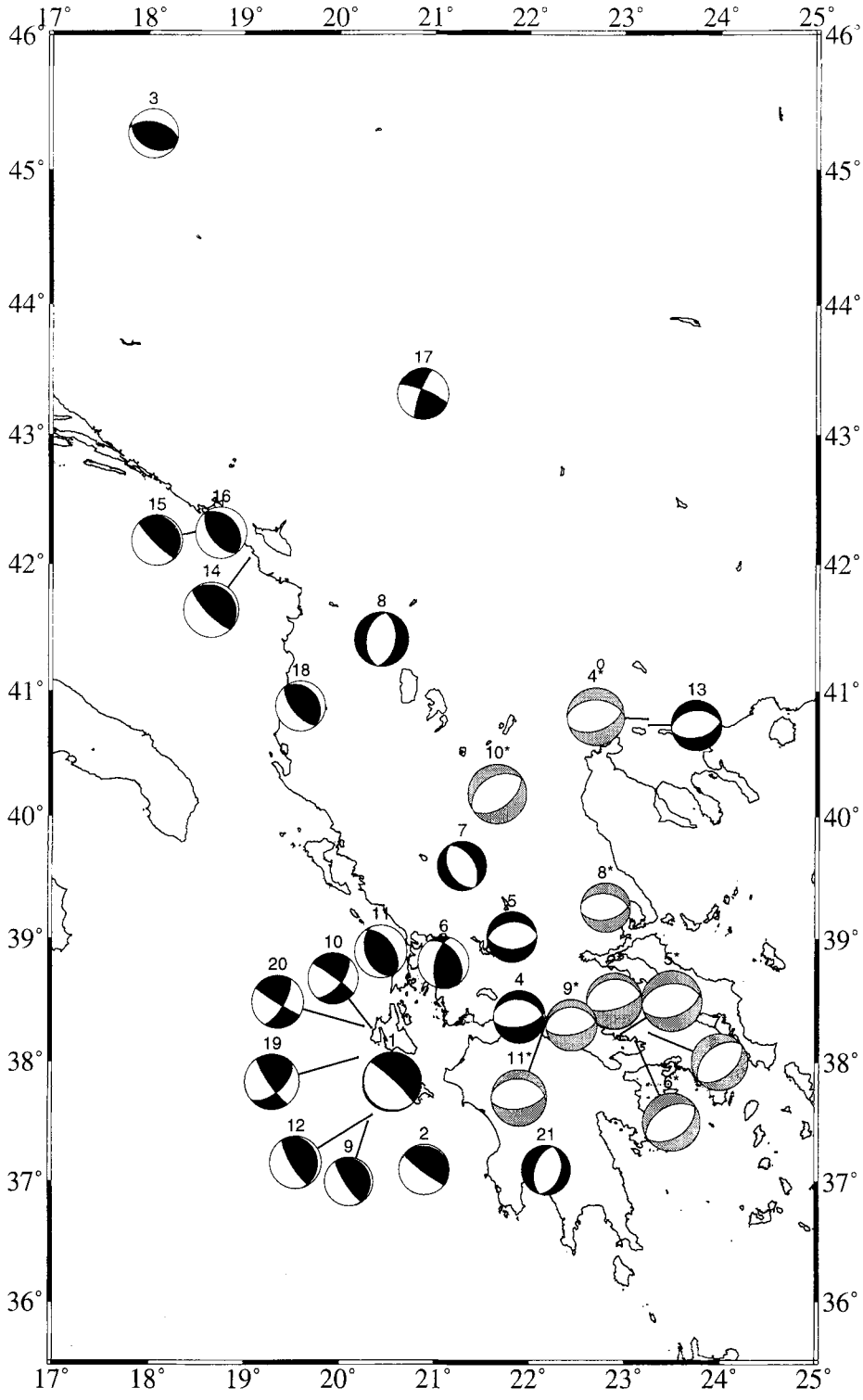

Figure 2. Map of the shallow ($z < 50$ km) mechanisms computed from body-wave modelling in the western Aegean. The two subcrustal-depth earthquakes (events 1* and 3*) are not reported.

and QUE (line 3, Fig. A3b). A strike-slip mechanism (line 4, Fig. A3b), similar to that found for the other earthquakes studied in this region (Anderson & Jackson 1987), can be ruled out on the basis of the relative *P* and *SH* amplitudes. Thus it is possible to distinguish between a strike-slip and a dip-slip solution, but the poor coverage of stations with available *SH* waveforms means that the orientation (and in particular the strike) of the resulting solution is not very well constrained (Table 1a and Fig. A3b).

Three other events in this vicinity, which all show a large strike-slip component, were also investigated by Anderson & Jackson (1987). However, these strike-slip solutions are not very well constrained and could be drawn as thrust-faulting-type events, violating only one polarity in each case. There is

Downloaded from http://gji.oxfordjournals.org/ at Observatoire de la CÃ'te d'Azur - Geoazur on December 13, 2016

therefore no clear inconsistency between our solution and other solutions for the same area, and, if we consider the north-dipping plane to be the fault plane for these events, the orientation of the faults is similar to the young structural features mapped in this region (Philip 1983).

1967 November 30, event 8, Fig. A8

This earthquake occurred in central Albania and shows normal faulting with nodal planes trending NE–SW. The first-motion polarities (Anderson & Jackson 1987) constrain the nodal plane trending N200° and dipping west quite well, but not the other plane. While the *P* waveforms do not constrain the nodal-plane orientations well, the *SH* waveforms provide good constraints. Sulstarova & Kociaj (1980) made a field study of this earthquake. The strike of the 10 km surface faulting (N40°E), the orientation and shape of the macroseismic field and the distribution of aftershocks are roughly in agreement with our solution. Sulstarova & Kociaj (1980) suggested that the active fault plane dips to the east.

Fig. A8(b) shows the variation in fit of the waveforms for a range of different models. Line 1 shows the minimum-misfit solution. Line 2 shows the model of Sulstarova & Kociaj (1980) deduced from the first-motion readings of *P* and *PKP* phases reported in the ISC bulletins [and different from the solution of Anderson & Jackson (1987), which is shown in Line 3]. However, as these readings are often taken from the short-period records, they may be inaccurate. It can be seen that the amplitudes of the *P* waveforms at AAE and WIN are clearly incompatible with those observed. Line 3 shows the solution of Anderson & Jackson (1987). This is not dissimilar to our solution, but the fits for the *SH* waveforms at CHG, NDI and WIN are noticeably less good. Lines 4 and 5 investigate how well we can constrain the strike from the available waveforms. In each case the strike is fixed at its given value and the other parameters are allowed to vary freely. These show, mainly from the deterioration in the fit of the *SH* waveforms at CHG, AAE and WIN, that the strike may vary by $\pm 25°$ from the minimum-misfit solution. The mechanism shows normal faulting, as seen for the Kozani event of 1995 May 13 (Hatzfeld *et al.* 1997). However, the trend of the T-axis is more E–W than that of the Kozani event.

1979 April 15, 06:19 hr, event 14, Fig. A14

This very destructive event, known as the Montenegro earthquake, is one of the largest (magnitude 6.7) events to have occurred in this region. It has been studied by several authors (e.g. Academy of Sciences of Albania 1983; Console & Favali 1981; Sulstarova 1980). It was part of a long seismic sequence lasting several months starting in March 1979. The aftershock sequence is complex and exhibits two dense clusters separated by a gap of about 20 km located offshore. The accuracy of the aftershock locations is not precise enough to infer the active fault, but there is some indication that the NE shallow-dipping plane is the fault plane, and this is consistent with tectonics observations (Tagari 1993). Fault-plane solutions have also been computed, by several authors using several methods (e.g. Boore *et al.* 1981; Giardini *et al.* 1984; Kanamori & Given 1981; Anderson & Jackson 1987). These solutions show a pure thrust fault on NW–SE-striking nodal planes with one very shallow NE-dipping plane. Our minimum-misfit solution shows a similar orientation and dip for the steeper nodal plane, with a significant strike-slip component. Fig. A14(b) shows a solution with a pure dip-slip mechanism and we observe a comparable fit of the waveforms. It confirms that the east-dipping plane is poorly constrained and therefore we prefer the solution showing pure dip-slip faulting, which agrees better with the tectonics of the area.

The ISC suggested that the event may have been multiple, that is formed by the superposition of a number of smaller subevents separated either in time or in space. This view, supported by the seismic moment estimated with long-period body waves, disagrees with the one concerning data computed from Rayleigh waves. There is evidence of complexity at stations in the NW part of the focal sphere, with a strong secondary arrival at stations in northern Europe and the US. However, we have been unable to find a multiple mechanism which fits these secondary arrivals and maintains an adequate fit at other stations. Our solution indicates that a single event with a fairly complex rupture–time history adequately matches the observed waveforms at most stations, and in the absence of other evidence we prefer this solution.

1979 April 15, 14:43 hr, event 15, Fig. A15

This event occurred just to the west of the Montenegran Coast, in the same area as the previous event (event 18) and on the same day and is the largest aftershock of the sequence. The minimum-misfit solution from waveform modelling and the solution from first-motion readings (Anderson & Jackson 1987) are very similar. There is therefore no need for further tests for this event. The fault-plane solution shows a thrust fault on NW–SE-striking nodal planes, similar to the previous mechanism. The NE-dipping nodal plane has a very shallow dip, but again its orientation is poorly constrained. The steeper plane is primarily constrained by the small-amplitude nodal character of the *P* waveform at NAI. The poor amplitude fit of the *SH* waveform at CHG suggests that the magnification reported for this station is incorrect, but we could find no independent evidence for this. The *P* waveform at COL has an unusual shape. The original record was rather faint and it may have been incorrectly digitized or contaminated with noise. We have chosen to exclude this station from the inversion (it is marked with a star to indicate this).

1979 May 24, event 16, Fig. A16

This was the third earthquake in 1979 on the coast of the former Yugoslavia and also an aftershock of the previous sequence. Again, the minimum-misfit solution shows thrust faulting on a NW–SE-striking nodal plane with a small component of strike-slip motion. The solution obtained by Anderson & Jackson (1987) from first motions has a mechanism similar to the two events of 1979 April 15 (events 18 and 19), with one shallow NE-dipping plane striking parallel to the coast. The equivalent nodal plane in our minimum-misfit solution has a steeper dip towards the NNE, although this plane is poorly constrained by the available waveform coverage. The large, clear *P* waveforms observed at NAI, AAE, BUL and PRE, especially when compared to those seen for the April 15 events at the same stations, suggest the mechanism for this event is rather different: the SW-dipping plane is shallower than for the Montenegran events. The stations to

Downloaded from http://gji.oxfordjournals.org/ at Observatoire de la CÃ´te d'Azur - Geoazur on December 13, 2016

the south show some complications in the waveforms which we have been unable to match. These may reflect source-region heterogeneity or directivity effects. Interestingly, similar complications at these stations are observed in other studies of events in the Aegean and Adriatic (e.g. Barker & Langston 1981). Fig. A16(b) shows a pure dip-slip solution with the same strike and dip for the W-trending plane. The fits to waveforms for this solution are not perceptibly different from those for the minimum-misfit solution. Fig. A16(c) (Line 2) shows the waveform fits for the mechanism of Anderson & Jackson (1987), which shows a shallower NE-dipping plane. The amplitudes at African and North American stations are worse. Our preferred solution is therefore the pure dip-slip solution that differs from the others in the Montenegro group in having a steeper NE-dipping nodal plane.

1980 May 18, event 17, Fig. A17

This event is located in the former Yugoslavia. It is one of a number of events which occurred inland from the coast. The minimum-misfit solution (and our preferred solution) shows a strike-slip mechanism. The first motions alone cannot be used to distinguish between a thrust and a strike-slip solution (Anderson & Jackson 1987). The good coverage of *SH* waveforms allows us to show that the strike-slip solution is correct. A test plot (Fig. A17b, line 2) with a thrust mechanism similar to the Montenegran events (events 14 and 15) is clearly incompatible with the *P* and *SH* waveforms. There is no surface expression of the fault associated with this event, although most of the structural lineations in this area show a NW–SE strike (Anderson & Jackson 1987). This strike-slip earthquake is located near the Scutari-Pec strike-slip transform zone, which is thought to be an important geological boundary, but the trend of the inferred fault plane (203°) is more N–S than expected from the Scutari-Pec transform zone. This trend is relatively well constrained by the change in *P*-wave polarities at stations NDI, AAE, GDH and BLA.

1982 November 16, event 18, Fig. A18

This event occurred on the coast of Albania, south of the area affected by the Yugoslavian earthquakes of April and May 1979. The event was small ($M_b = 5.6$) and only a few waveforms are available. The mechanism shows pure thrust faulting with nodal planes striking NW–SE. The NE-dipping nodal plane is fairly shallow (30°), a little steeper than the events on the Yugoslavian coast. The poor focal-sphere coverage means that this solution is poorly constrained. Anderson & Jackson (1987) could not draw a solution from the first-motion polarities, but the solution is consistent with the one computed by Giardini *et al.* (1984).

3.2 Ionian Sea zone

1959 November 15, event 1, Fig. A1

The epicentre of this earthquake is located off the west coast of the island of Zakynthos (Papazachos *et al.* 1982). As the event occurred before the installation of the WWSSN was completed, there are rather few stations with which to constrain the solution, and the amplification of the stations is not well known, so we rely more on relative amplitudes between *P* and *SH* than on absolute amplitudes. A reasonable azimuthal coverage is nonetheless obtained. The rather small amplitudes of the *P* waveforms compared to the *SH* waveforms suggest nodal arrivals at AGR and PAL, and these constrain the NW–SE-striking plane well. The shallower-dipping plane striking NE–SW is poorly constrained. This plane is rather important as, depending on its orientation, the mechanism of this earthquake may correspond to a pure thrust, as seen along the line of the Hellenic Trench (events 2 and 10) or to an event showing some dextral strike-slip faulting, as seen for events along the Kefallinian Trough (e.g. events 13, 23 and 24). McKenzie (1972) drew the plane with a strike of 66°, but this azimuth is not constrained by any polarity. The minimum-misfit solution shows a significant right-lateral strike-slip component, assuming the NE–SW nodal plane to be the fault plane. In Fig. A1(c) we investigate the orientation of this NE–SW-trending plane. Line 2 shows the waveform match for *P* and *SH* waveforms at three stations for the minimum-misfit solution. The other lines show the waveform fits when the NE–SW-striking nodal plane is fixed at a different dip from that in the minimum-misfit solution and the other parameters are allowed to vary in the inversion. We can see that while the fits for the *SH* waveforms at LWI and PAL are marginally less good, the *P*-waveform fit is not noticeably worse. A pure dip-slip solution (Fig. A1b) is our preferred solution based on the geographical location and the mechanisms for events nearby. The dip of the shallow-dipping plane is certainly not constrained within 20° and could dip toward the east as neighbouring mechanisms do.

1963 December 16, event 2, Fig. A2

This earthquake is located to the south of the island of Zakynthos. The minimum-misfit solution shows a predominantly thrust solution on an E–W-striking fault plane, but there are only a few small *P* waveforms with which to constrain the solution, due to their poor signal-to-noise ratio and nodal nature (NAI and AAE). The focal mechanism drawn only with the first-motion polarities from long-period records is likely to be a dip-slip mechanism, but the azimuth of the vertical plane is not well constrained. McKenzie (1972) chose an E–W-striking plane, while Anderson & Jackson (1987) reported a NE–SW-striking fault plane. The strike is therefore in good agreement with the local trends in the bathymetry, and different from that proposed by Anderson & Jackson (1987). In Fig. A2(c), we test other solutions. Line 2 is for the nodal plane that strikes 127° parallel to the local bathymetry trends. While the fits for the *P* waves at CHG and QUE are marginally worse, the fit of the *SH* waves is fairly good. A strike of 147° does not fit the amplitudes well (line 3, Fig. A2c). This is also true (Line 4) of the solution of Anderson & Jackson (1987). Our preferred solution is therefore the one shown in Fig. A2(b) with a N127°-striking plane, consistent with the local trend of the Hellenic trench.

1966 October 29, event 6, Fig. A6

The ISC location for this earthquake is in Western Greece, to the SE of the Gulf of Arta. Intensities of VIII were observed in the Katouna valley (Papazachos *et al.* 1982; Papazachos & Papazachou 1989). Ambraseys (1975) reported between 2 and 4 km of surface faulting, with a NNW strike, that may be

Downloaded from http://gji.oxfordjournals.org/ at Observatoire de la CÃ´te d'Azur - Geoazur on December 13, 2016

associated with this event, and Papazachos & Papazachou (1989) mentioned surface cracks about 2 km long and 1–2 cm wide near Amphilohia.

There is a reasonable coverage of data for this event, but many of the stations in the NW quadrant of the focal sphere (in northern Europe and North America) lie on, or close to, the *P* node of the west-dipping plane. As a result, the signal-to-noise ratio for the first arrival may be rather poor, which may explain why it is hard to match the initial parts of these waveforms well at all stations. The minimum-misfit fault-plane solution is similar to that derived from first-motion readings by Anderson & Jackson (1987), although the strike of the shallow-dipping plane in our solution is rotated by about 20°. The NNE-striking plane dipping west is well determined by first-motion polarities both in strike and dip (Anderson & Jackson 1987), but the other shallow-dipping plane is not. Fig. A6(c) shows the effect of varying the strike on the resulting waveform fits. In each case, the strike is fixed at the given value (first figure in the line above each focal-sphere pair) and the other parameters are allowed to vary freely. Line 1 shows the fit for the minimum-misfit solution. Line 3 shows the fit when the nodal planes are rotated 30° anticlockwise. It can be seen that while the *P*-waveform fits are of similar quality, the amplitudes of the *SH* waveforms at the three stations show some deterioration. The fit of the amplitudes when the nodal planes are rotated 15° clockwise deteriorates (line 4, Fig. A6c). The uncertainties on the strike of the nodal planes of this event are therefore $-30°/+15°$. Our preferred solution is given in line 2 and displayed in detail in Fig. A6(b). It is similar to the solution of Anderson & Jackson (1987) given in line 5 of Fig. A6(c). The strike-slip component is smaller and the strike of the fault planes is closer to the one of the Katouna valley and to the surface breaks reported by Ambraseys (1975).

We also considered solutions showing pure reverse mechanisms, with the *P*-axis trending NE–SW as for the reverse solutions in western Greece, or pure strike-slip motion as observed west of Kefallinia. They show a worse fit to the data in both cases. This mechanism, which does not fit tectonic or microearthquake observations, and which is different from the Ionian islands mechanisms, is rather puzzling.

1969 July 8, event 9, Fig. A9

This event lies southwest of Zakynthos. The epicentre is in an area where the depth of water is around 3000 m. Studies using first motions of long-period *P* waveforms by McKenzie (1972) and Anderson & Jackson (1987) give a focal mechanism with one near-vertical fault plane whose strike is well constrained and one rather poorly constrained, shallow-dipping plane. Despite the relatively small magnitude of this event ($m_b = 5.4$), it is well recorded teleseismically and there is a good station coverage from which to model the event. The small amplitudes of the *P* waveforms at NAI and AAE contribute to the constraint of the steeply dipping nodal plane, but not to the poorly constrained, shallow-dipping plane. The strike of the nodal planes is parallel to the strike of the Hellenic Trench in this region. The mechanism proposed here is not very different from the mechanism of Anderson & Jackson (1987).

1972 September 17, event 10, Fig. A10

This event occurred just off the west coast of Kefallinia and is well recorded teleseismically. The minimum-misfit solution corresponds to a strike-slip solution with a shallow centroid depth (6 km ± 4). The SW-dipping nodal plane is parallel to the local trend of the isobaths. Our solution is similar to that obtained by Anderson & Jackson (1987) from long-period *P*-wave first motions, but different from the first solution proposed with only a few readings by McKenzie (1978). The good focal coverage of *P* and *SH* waveforms ensures a well-constrained solution, especially for the NW–SE striking plane.

A number of the stations in the west show strong secondary arrivals on the *P* waveforms (e.g. PDA, BEC, BLA, SCP) delayed by about 11 s with respect to the first motion. We can find no realistic model which accounts for this arrival and maintains a reasonable fit to the waveforms at stations in other parts of the focal sphere. These features may result from near-source structural effects, path effects or source directivity which we are unable to match adequately with our model.

1973 November 4, event 11, Fig. A11

This event is located off the coast of NW Greece. The event of magnitude 5.8 is rather small (close to the lower limit for use in body-waveform modelling) and the single *P* waveform clearly gives no constraint on the orientation of the nodal planes. However, the *SH* waveforms provide an adequate constraint on the nodal-plane orientation. Anderson & Jackson (1987) show two alternative solutions for this event, based on first-motion readings from long-period seismograms at teleseismic and regional distances, which we tested in Fig. A11. The first, a thrust mechanism, is almost identical to our minimum-misfit solution. The second (Fig. A11b, line 2) has a predominantly strike-slip mechanism and can be shown to be incompatible with the observed *SH* phases. The dip of the NE-dipping plane is relatively well constrained. We try a dip of 35° (Fig. A11b, line 3) that increases the misfit in most of the stations. A dip greater than 45° is therefore very likely, significantly greater than that observed for both the Montenegran events located to the north, and the trench events located to the south. The depth given by the minimum-misfit solution is 23 km, which is somewhat deeper than the other thrusting mechanisms along the NW Greek, Albanian and Yugoslavian coasts. This is not very well constrained by the single weak *P* waveform, so the error on this depth is greater than the ±3 km which is commonly found from this type of modelling. A test made with a shallower depth (Fig. A11b, line 4) causes a slight increase in the misfit at SHL and NDI, which show a smaller amplitude than that observed. The seismic moment is larger in this model, but otherwise the mechanism remains similar to the minimum-misfit solution. It is likely, therefore, that the focal mechanism is a reverse-faulting one, the *P*-axis trending NE.

1976 May 11, event 12, Fig. A12

The epicentre of this earthquake is located near to that of the 1969 July 8 event (see above), where the water depth reached 4000 m. Several of the waveforms for this event were obscured by the surface waves of another earthquake which occurred 1 hr before. The waveforms which were available, however, still provided an adequate focal-sphere coverage to give a well-constrained solution. The minimum-misfit solution shows a predominantly thrust-faulting mechanism. This is similar to that obtained by Anderson & Jackson (1987), although our

Downloaded from http://gji.oxfordjournals.org/ at Observatoire de la CÃ´te d'Azur - Geoazur on December 13, 2016

solution requires a steeper dip for the NE shallow-dipping nodal plane, which is rather poorly constrained in both models. A pure dip-slip solution (Fig. A12b), with planes striking parallel to the trench, fits the observations equally well, and this is the solution that we adopt. The source time function has a duration of about 8 s, and the centroid depth is 12 km.

1983 January 17, event 19, Fig. A19

This is one of the largest earthquakes ($M_s = 7.0$) to have occurred in the area studied and has been the subject of several investigations. This epicentre lies SW of the island of Kefallinia in an area which had been identified as a seismic gap before its occurrence (Papadimitriou & Papazachos 1985).

Using long- and short-period data, Scordilis *et al.* (1985) suggested a right-lateral strike-slip mechanism with a small thrust component on a fault plane with a NE–SW strike. Their choice of nodal plane was supported by the locations of the large number of aftershocks which occurred. Anderson & Jackson (1987) concluded that a thrust solution provided a better fit to the available data, basing their solution on first motions of long-period *P* waveforms. The Harvard CMT solution (Dziewonski, Friedman & Woodhouse 1983) shows a thrusting mechanism indicating NE–SW compression (perpendicular to the trend of the Hellenic Trench) at a depth of 10 km.

Attempts at body-waveform modelling by a number of authors (Bezzeghoud 1986; Papadimitriou 1988; Ioannidou 1989; Kiratzi & Langston 1991) favour the strike-slip solution. There is a good coverage of *P* and *SH* waveforms with which to constrain the solution, which corresponds to strike-slip faulting with a thrust component. The position of the NW–SE-striking nodal plane is constrained by the dilatational first motions at BUL, SLR and SJG and the compressional first motions at GOL, LON and DUG. Several of the stations between have rather nodal onsets, but our model fails to match the whole waveform adequately. The dip of the NE–SW-striking plane is not as well constrained by the *P* waveforms and is likely to be in the range 45°–60°. However, a pure reverse solution is shown in Fig. A19(b) and fits the seismograms equally well for most of the stations and even better for *SH* waves at stations SLR and BUL. It is impossible to decide, on the basis of the best fit only, on the most likely solution, and we consider the strike-slip mechanism to be the fault plane on the basis of the aftershock pattern and its correlation with the local bathymetry.

1983 March 23, event 20, Fig. A20

The epicentre of this event lies very close to the location of the 1972 September 17 and 1983 January 17 events. It is the largest aftershock of this latter event. It can be seen that the *P* waveforms are rather noisy, but the coverage is good and the *SH* waveforms help to constrain the solution. The mechanism is similar to the two other events, showing a strike-slip fault with a thrust component. The nodal waveforms at WES help to constrain the NW–SE-striking nodal plane. The SW–NE nodal plane (the probable fault plane) is, however, less well constrained. The poor signal-to-noise ratio of the *P* waveforms means that the depth (minimum-misfit solution value of 6 km) is also poorly constrained for this event. A number of stations (TRN, CAR and SJG) show phases within the *P* waveform which we are unable to match with our model. These may be the result of lateral heterogeneity in the near-source structure. We have opted to weight these to zero (they are thus marked with a star) in the inversion and include them in Fig. A20 to show that they are different in form to the other *P* waveforms for this event. Our solution is very close to that obtained by Anderson & Jackson (1987) and to the other mechanisms computed in the same area.

3.3 Central Greece

1965 July 6, event 4, Fig. A4

This earthquake is located on the northern side of the Gulf of Corinth, to the west of the region affected by the 1981 earthquake sequence (Jackson *et al.* 1982; King *et al.* 1985). This shock probably occurred within the Gulf of Corinth, but was not followed by a significant sequence of aftershocks (Ambraseys & Jackson 1990), as was observed for the Galaxidi earthquake of 1992 December (Hatzfeld 1996). A mechanism has been computed by McKenzie (1972) who proposed a shallow plane dipping north at 14°, but it was computed with a mantle velocity structure at the focus. Jackson & White (1989) recomputed the mechanism with a crustal velocity structure. Their solution is not a pure normal fault as found here, but we do not have the readings necessary to check them. The minimum-misfit solution (Fig. A4a) shows two E–W-striking nodal planes. The first, dipping north, has a shallow dip (33°), while the other dips south rather more steeply (58°). For this event, we show the full range of diagrams which were used to test the uncertainties on the individual source parameters, using the approach outlined in Section 3.

In each diagram (A4 b,c,d and e) the top line shows the fit obtained at six station/phase pairs for the minimum-misfit solution. Subsequent lines show the fit achieved when the parameter under test is fixed at a range of values different from that of the minimum-misfit solution, while the other parameters are allowed to vary freely. For example, Fig A4(b) shows the test for the uncertainty in strike for this earthquake. The second line shows the fit obtained when the strike is fixed at 55° (24° anticlockwise from the minimum-misfit solution). Here we can see that the fit is worse (marked with a vertical bar) for the *SH* phase at AAE (incorrect sense of first motion), WIN (amplitude too large) and WES (amplitude too small). The amplitude is also slightly larger than the observed signal for the *SH* phase at NDI. Note that the fit at one station is better than that obtained for the minimum-misfit solution (the *P* wave at QUE which is marked with an asterisk). It is not uncommon (e.g. Taymaz *et al.* 1991) for the fit at one station to improve when a parameter is fixed at a value that can be considered unacceptable because of the poor fits at several other stations (or indeed a different phase at the same station). Line 3 shows the fit obtained when the strike is fixed at 65°. In this case the misfit of the *SH* phase at AAE is less severe as the strike is closer to that of the minimum-misfit solution, although there is still a slight deterioration to the fit of the phases at WIN and WES. Lines 4 and 5 in this diagram show how the fit deteriorates when the strike is varied to values of 90° and 100°. There is a slight deterioration of the fits at 90° and a more convincing deterioration at 100°. From these results we conclude that the strike of this event is constrained to around ±25°. The other diagrams in this set give us the

Downloaded from http://gji.oxfordjournals.org/ at Observatoire de la CÃ´te d'Azur - Geoazur on December 13, 2016

uncertainties in the dip, rake and depth values obtained for the minimum-misfit solution.

Line 3 in Fig. A4(c) shows the fit when the dip of the southerly dipping nodal plane is fixed at a shallower value, similar to that obtained from modelling of the 1981 Corinth sequence (Taymaz *et al.* 1991). This nodal plane is well constrained by the *SH* waveforms at NDI and KEV and the first-motion readings at AAE and WIN which, although close to the nodal plane, show a fit which is clearly less good if the shallower dip is used. The mechanism is similar to the mechanism (event 9*, Fig. 2) of the Galaxidi earthquake of 1992 November 18 (Briole *et al.* 1993; Hatzfeld *et al.* 1996).

1966 February 5, event 5, Fig. A5

This earthquake is important because it is located in Central Greece in a region where the level of seismicity is relatively low, as can readily be seen from the map of CMT solutions between 1980 and 1992 (Fig. 3). It is located close to the Kremasta Dam in western Greece, and is thought to be associated with the filling of this reservoir. The event was investigated by McKenzie (1972), Fitch & Muirhead (1974), Stein, Wiens & Fijita (1982) and Anderson & Jackson (1987) using first-motion polarities. The north-dipping nodal plane is rather well constrained by first-motion polarities. The poor station coverage available for waveforms means that this solution is not well constrained, and only three rather noisy *SH* waveforms are available which do not help in fixing the second plane. The minimum-misfit solution (Fig. A5a) corresponds to a normal fault with E–W-striking nodal planes, and is similar to that obtained by Anderson & Jackson (1987). Fig. A5(b) shows the minimum misfit (line 1) in comparison with the solution proposed by Anderson & Jackson (1987) (line 2). The orientation and the dip of the southerly dipping plane is well constrained by the *SH* waveforms at NAI and PRE.

1967 May 1, event 7, Fig. A7

This earthquake of magnitude 6.4 lies in NW Greece, inland from the coast, west of the Pindus mountains. It resulted in some damage to a dozen villages (Ambraseys & Jackson 1990). It has a normal-faulting mechanism with a NNW–SSE strike. No surface break was reported for this earthquake. Some regional first-motion readings (Anderson & Jackson 1987) provide additional data that constrain the mechanism better. This additional information is needed in this case, as the waveforms alone do not constrain the mechanism sufficiently well. The mechanism we obtain for this earthquake is shown in Fig. A7(a). Fig. A7(b) compares the fits for this minimum-misfit mechanism (line 1) with those of other possible mechanisms. Line 2 shows the waveform fit obtained using the fault-plane solution of Anderson & Jackson (1987) using first-motion polarities alone. This clearly gives a less good fit to the *SH* waveforms at LAH, AAE and GDH. The discrepancy between the mechanism obtained by first-motion readings alone and that obtained from inversion of the body waves may reflect a change in the orientation of the rupture during the time-history of the event. Lines 3 and 4 of Fig. A7(b) show the fit when the strike is fixed at $-30°$ and $+30°$, respectively. This shows that while the *P*-waveform fits are not sensitive to this change in strike, the *SH* waveforms show significant deterioration at these extreme values. Unfortunately, compared to the *P* waveforms, the *SH* waveforms have a poor signal-to-noise ratio and it is difficult to constrain the orientation of the nodal planes for this event. Nevertheless, it seems that this event indicates the existence of normal faulting with near-NNW–SSE-striking features, rather than E–W-striking faults as seen to the south (Gulf of Corinth sequence, Taymaz *et al.* 1991) or central and eastern Greece.

1978 May 23, event 13, Fig. A13

This event occurred in the NE of Greece near to the city of Thessaloniki. It occurred in the same area and one month before the 1978 June 20 event ($M_s = 6.4$). The mechanism of this foreshock has been studied by several authors (Papazachos *et al.* 1979; Soufleris & Stewart 1981). It is constrained primarily by a few rather noisy *SH* waveforms at KEV, AAE and NAI and shows nearly pure normal faulting on E–W-striking nodal planes, which is consistent with the polarities of the first motions. It is also similar in orientation and depth to that obtained from the body-waveform modelling of the 1978 June event (Soufleris & Stewart 1981; Barker & Langston 1981; Liotier 1989) and is very probably associated with a fault plane dipping north, as inferred by surface faulting observed during the main shock (Papazachos *et al.* 1979; Mercier *et al.* 1979, 1983).

1986 September 13, event 21, Fig. A21

This event is located in the southern part of the Peloponnese, near Kalamata (Papazachos *et al.* 1988). In spite of its moderate magnitude of 5.8, this earthquake caused considerable damage. It is of particular interest since there are few available mechanisms in the southern part of the Hellenic arc between the Ionian islands and Crete. The Harvard CMT solution shows a normal fault with a strike-slip component on N–S-striking nodal planes. Lyon-Caen *et al.* (1988) made an extensive study of this earthquake, including tectonic observations, body-wave modelling and an aftershock study. Our minimum-misfit solution is very similar to the solution proposed by Lyon-Caen *et al.* (1988). This shows a normal fault on N–S-striking nodal planes, but with little or no strike-slip component, and is well constrained by the few *SH* waveforms.

4 INTERPRETATION AND DISCUSSION

The 21 focal mechanisms that we modelled and the 11 modelled by others are shown in Fig. 2. We also show the 79 CMT solutions computed between 1977 and 1995 for the same area in Fig. 3. These two figures show a complex picture including reverse, normal and strike-slip faulting, which we will discuss in the following sections.

4.1 Subcrustal-depth earthquakes

Within the Aegean, the subcrustal seismicity is mostly located beneath the sea of Crete. It is not frequent beneath the northwestern part of the Hellenic arc. No reliable mechanisms at that depth have been computed by modelling body waves because the events are of relatively low magnitude.

The first event considered in this study occurred on 1965 March 31 and is located at a depth of 55 km beneath the

Downloaded from http://gji.oxfordjournals.org/ at Observatoire de la CÃ'te d'Azur - Geoazur on December 13, 2016

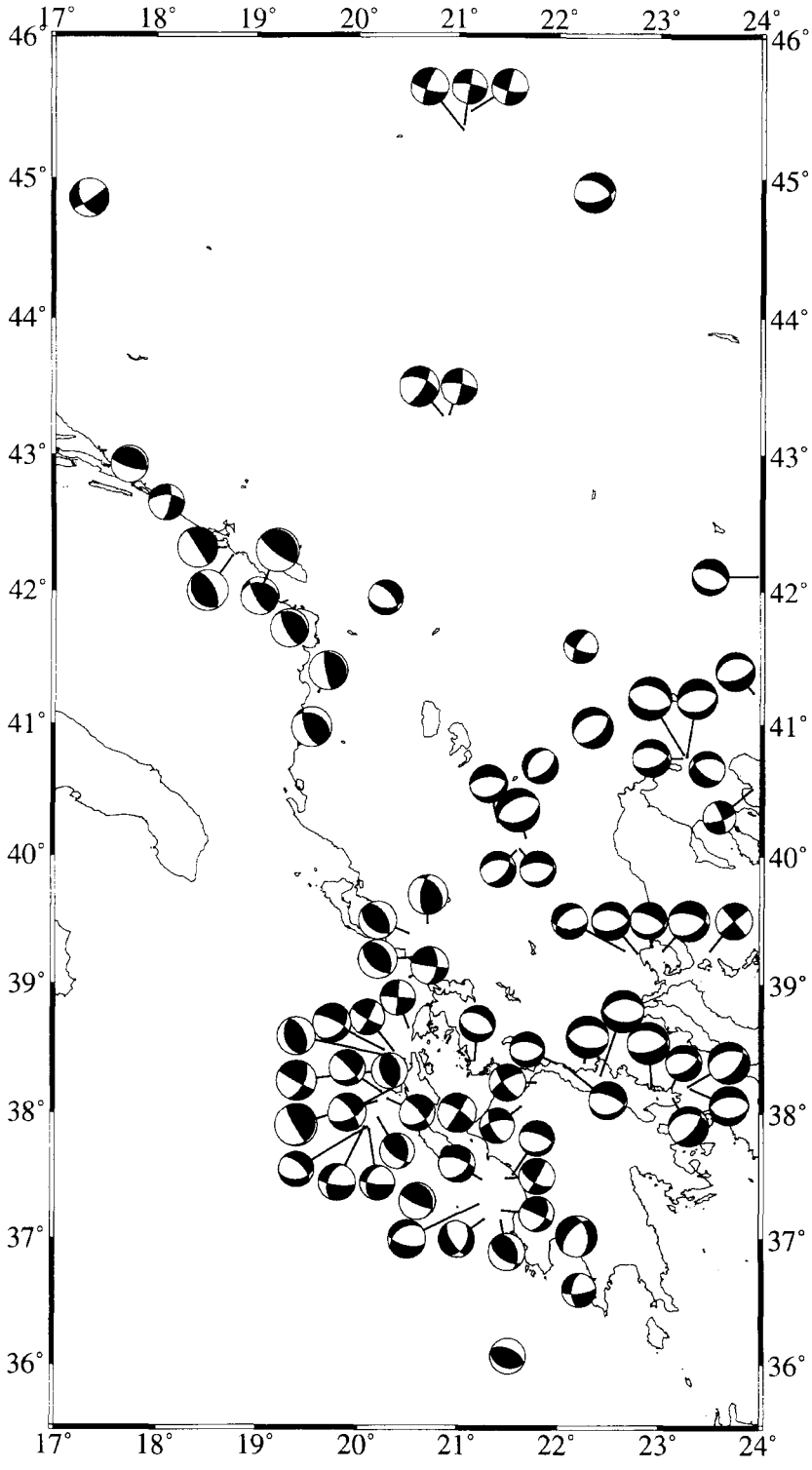

Figure 3. Map of the shallow ($z < 50$ km) CMT solutions that are available in the western Aegean.

Gulf of Corinth (event 1*, Table 1b). The depth is well determined by modelling (Liotier 1989) and confirms the uncertain subcrustal depth given by the ISC, USGS and BCIS. The reported location of the epicentre differs by as much as 50 km from one agency to another and the macroseimic observations suggest a location beneath Patras or to the east of it. The mechanism shows reverse faulting with the *P*-axis trending ENE and the *T*-axis nearly vertical, which is consistent with the few subcrustal-depth microearthquake mechanisms computed in this area (Hatzfeld *et al.* 1989). The event is most probably related to the beginning of the steep part of the subducted slab beneath the Peloponnese and supports the idea that this slab dips gently for the first 200 km before dipping more steeply beneath the Gulf of Corinth (Hatzfeld *et al.* 1989).

The second subcrustal-depth event (event 3b*, Table 1b) occurred on 1972 September 13, and is located at a depth of

Downloaded from http://gji.oxfordjournals.org/ at Observatoire de la CÃ´te d'Azur - Geoazur on December 13, 2016

79 km. In this case the accuracy of the epicentre, north of the Peloponnese and east of the previous earthquake, is better. The depth is quite well determined by modelling (Liotier 1989). The mechanism shows strike-slip motion, with a slight component of reverse faulting. This mechanism is not really consistent with any of the reliable mechanisms that we know of for subcrustal earthquakes associated with Hellenic subduction. It is probably located at the base of the overriding lithosphere and not related to the pull of the dipping slab itself.

4.2 Normal faulting

Normal faulting is associated with the internal part of the Aegean region and related to the important extension which prevails (McKenzie 1978). Our mechanism confirms and provides information on the direction of extension. We observe N–S extension on E–W-trending planes in northern Greece (events 4* and 13), central Greece (events 5 and 8*), and the Gulf of Corinth (events 1*, 2*, 5*, 6*, 7*, 9* and 11*). Along the external part of the belt, the extension is trending more E–W to WNW–ESE, as seen in Albania (event 8), Macedonia (event 10*) and the southern Peloponnese (event 21).

This pattern of extension is consistent with mechanisms computed for microearthquakes (Hatzfeld *et al.* 1987, 1990, 1995; Rigo *et al.* 1996) and roughly consistent with most of the tectonic observations made in Albania (Tagari 1993), in Epirus (Waters 1993), in Akarnania (Sorel 1989) and in the Peloponnese (Mercier, Sorel & Simeakis 1987; Armijo, Lyon-Caen & Papanastassiou 1992; Armijo *et al.* 1996). Moreover, it is consistent with geodetic observations in the western Hellenic arc (Kahle *et al.* 1993; Noomen *et al.* 1994). It confirms that, within the Aegean domain, internally the extension is approximately N–S; close to the convergent boundary it is approximately parallel to this boundary.

4.3 Strike-slip faulting

Three mechanisms (events 10, 19, 20) located west of Kefallinia clearly show strike-slip motion. If the NE-striking plane is the fault plane, which is consistent with local tectonics, then the motion is right lateral and the trend of the slip vector is $37° \pm 12°$N, slightly different from that of the reverse mechanisms (Fig. 4). This is the area which experienced the strongest earthquakes in the recent past (Papazachos & Papazachou 1989). The tectonics show clear dextral strike-slip motion on the Kefallinia fault located west of Kefallinia (e.g. Cushing 1985; Sorel 1989), which is consistent with GPS geodetic observations (Kahle *et al.* 1993), with our mechanisms, and also with the mechanisms computed in this area for microearthquakes (Hatzfeld *et al.* 1995). However, it is unclear whether this affects a large or a narrow zone and if it is an active decoupling boundary for a rigid block (as suggested by Brooks *et al.* 1988 or Le Pichon *et al.* 1995) or only a transfer zone. Indeed, the motion (measured by GPS) relative to stable Europe increases away from the Kefallinia fault, which favours a rigid plate motion around a pole located near the Kefallinia fault, but this motion also affects central Greece. There are two arguments which support a distributed shear: (1) the strike-slip motion is limited in length, and affects only the Kefallinia fault, which does not continue in continental Greece; (2) the azimuth of the displacement of the Ionian islands relative to stable Europe (35°N) differs from the strike of the Kefallinia fault as given by the bathymetry (20°N). This difference should result in strike-slip mechanisms with a reverse component, which is not observed.

4.4 Reverse faulting

Reverse faulting is seen along the external part of the Hellenic arc. In Albania and northern Greece it is associated with continental collision, and south of the Ionian islands it is associated with active subduction. One event (event 3) is located in the former Yugoslavia and is likely to be related to the thrust of the Dinarides mountains beneath the Pannonian basin. Here the dip of the NE-dipping plane is 52°. One other event (event 6) is located in the continental domain but is inconsistent with other thrusting events along the NW Greek and Albanian coasts. It is inconsistent with the tectonic observations along the Katouna valley which clearly show a sinistral strike-slip transfer zone (Brooks *et al.* 1988; Sorel 1989; Underhill 1989). It is also inconsistent with the mechanisms of microearthquakes in this region, showing N–S extension (Hatzfeld *et al.* 1995).

Most of the other mechanisms show a very shallow-dipping plane toward the NE, and a *P*-axis trending NE. The dip of the inferred fault plane, like the trend of the *P*-axis (or of the slip vector), shows a remarkable consistency across the Ionian islands, independent of the type of convergence at the active boundary (oceanic subduction or continental collision). This type of shallow-dipping reverse mechanism is also present south of Crete but with a different trend for the slip vectors and a different centroid depth (Taymaz *et al.* 1990). South of Crete, the mean depth of events is about 35–40 km and the mean trend of the slip vector is about 20°. West of the Hellenic arc, the mean depth is about 10 km and the trend of the slip vectors is about 50°.

4.5 Discussion

The consistent trend for the slip vector, which is consistent with the homogeneous pattern of palaeomagnetic rotation from southern Peloponnese (Kissel & Laj 1988) to the former Yugoslavia (Speranza *et al.* 1995), does not support the idea of a rigid-type rotation of western Greece around a pole located near the boundary, as suggested by Le Pichon & Angelier (1979) and Le Pichon *et al.* (1995). The difference (30°) in the azimuth of the slip vector between the western part of the Hellenic arc and the area south of Crete [trending consistently 20°N (Taymaz *et al.* 1990)], assuming that both converge towards the same rigid African plate, is consistent with internal deformation within the Aegean, probably located between the southern Peloponnese and Crete (Hatzfeld *et al.* 1993).

The similarity of the mechanisms associated with continental collision in the north with those associated with active oceanic subduction in the south is remarkable. Shallow-dipping reverse mechanisms are common for subduction zones and are related to the motion of the overriding lithosphere. They are also seen in continental tectonics when they are related to active boundaries as in the Main Boundary Thrust (MBT) of the Himalaya (Molnar & Lyon-Caen 1989). However, usually for intraplate deformation, for example the Zagros mountains (Jackson & McKenzie 1984) or the eastern Cordillera of Peru and Bolivia (Suarez, Molnar & Burchfield 1983), the fault planes show

Downloaded from http://gji.oxfordjournals.org/ at Observatoire de la CÃ'te d'Azur - Geoazur on December 13, 2016

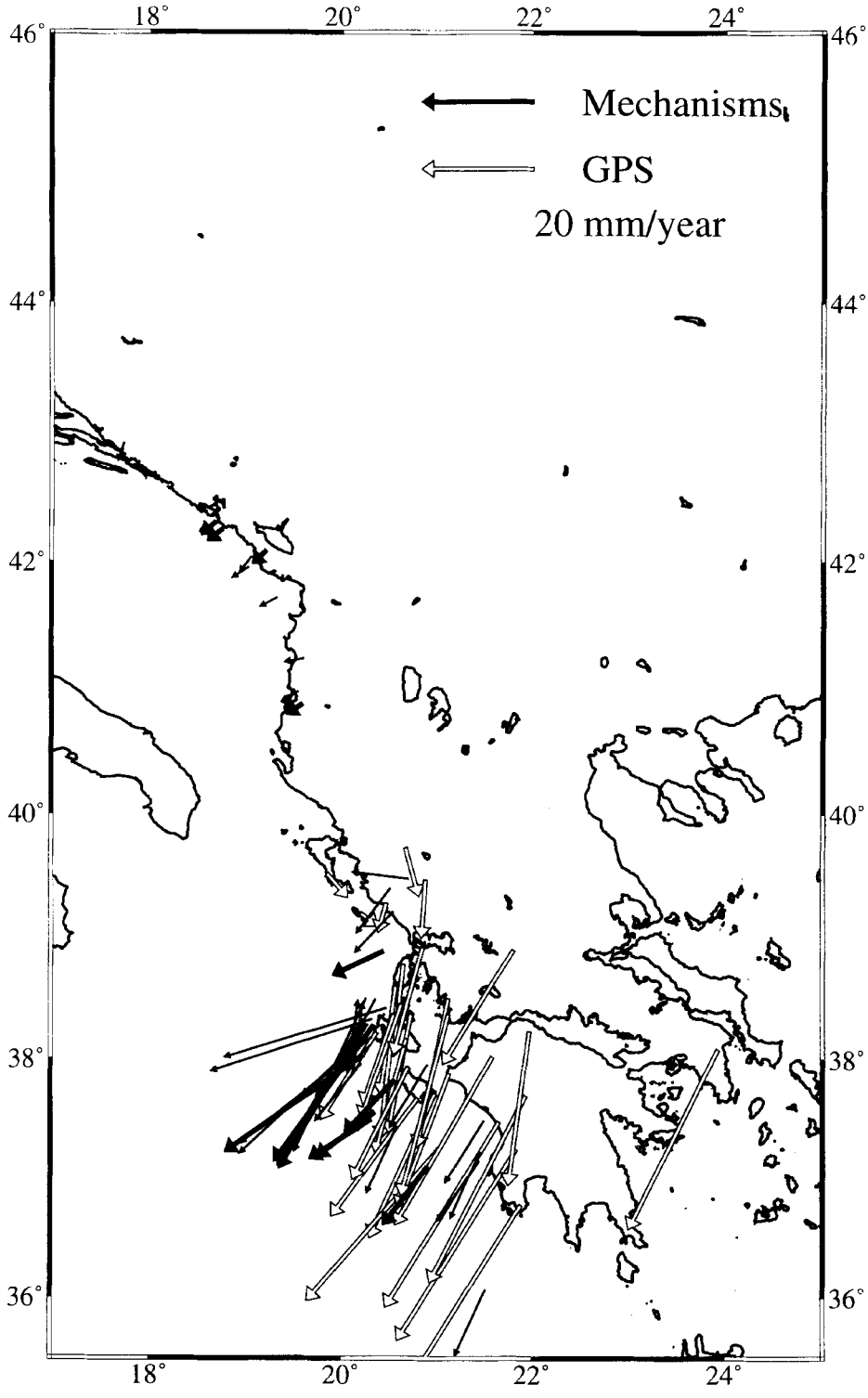

Figure 4. Map of the slip vectors and of the GPS displacement of western Greece relative to Africa (Table 3) deduced from Kahle *et al.* (1995). Heavy arrows are our focal solutions, thin arrows are CMT solutions, white arrows are GPS displacements. The slip vectors are sized by the annual scalar seismic moment rate (Papazachos & Kiratzi 1996). We have displayed only the mechanisms related to the active boundary and the CMT solutions showing reverse or strike-slip faulting.

steeper dips. The shallow-dipping reverse faulting that is present north of the Ionian islands suggests therefore that a major active boundary is located west of the Hellenides from the southern Peloponnese to northern Greece.

We report the horizontal projection of the slip vectors in Fig. 4 and Table 2. The mean trend of the slip vectors is $53° \pm 7°$N for the continental collision in the north and $47° \pm 9°$N for the oceanic subduction in the south. This difference in trend between continental collision and oceanic subduction is not significant and supports the idea that the seismic

Downloaded from http://gji.oxfordjournals.org/ at Observatoire de la CÃ'te d'Azur - Geoazur on December 13, 2016

Table 2. Azimuths of the slip vectors for the reverse mechanisms.

Region	Earthquake	Azimuth (°N)	Rate (mm yr^{-1})	mean
collision	11	248	10	232±9
	14	226	04	
	15	225		
	16	232		
	18	231		
subduction	1	223	13	227±9
	2	217		
	9	237		
	12	233		
Kefallinia	10	216	30	220±13
	19	235		
	20	211		

deformation of the Aegean is continuous from north Albania to the southern Peloponnese (Hatzfeld *et al.* 1995). According to Papazachos & Kiratzi (1996), the mean annual seismic scalar moment rate is about 2.23×10^{18} N m for northwestern Greece and 6.31×10^{18} N m for the Hellenic subduction from Kefallinia to Crete, or in other words the velocity relative to stable Africa, deduced from seismic energy release, is of the order of 0.35 cm yr^{-1} for continental collision and 1.3 cm yr^{-1} for Hellenic subduction (Papazachos & Kiratzi 1996). Thus the moment release is about 3–4 times greater for Hellenic subduction than for continental collision.

We also report the displacements relative to Africa deduced from the GPS measurements relative to Matera (Kahle *et al.* 1993), corrected from the motion of Matera relative to Europe (Le Pichon *et al.* 1995) and from the relative motion of Europe relative to Africa (Table 3 and Fig. 4). These values clearly show that the continental collision is related to a very small relative motion (less than 0.7 cm yr^{-1}) in the north, while the oceanic subduction is related to fast motion, relative to Africa, of about 3.5 cm yr^{-1} with an azimuth of 35°N in the Peloponnese (Kahle *et al.* 1995). Therefore, between the continental collision and the Hellenic subduction, the azimuth of the relative motion is very similar but the amplitude of the motion is very different.

There is, therefore, a marked difference between the information deduced from geodetic observations (related to differences in coordinates at the Earth's surface), and that deduced from earthquakes (related to seismic energy released within the crust). This leads us to several remarks.

(1) The azimuth of the GPS relative velocity is similar (within 20°) to that of the earthquakes' slip vectors. It is therefore likely that they are due to the same boundary condition, which is the actual motion of the Aegean relative to Europe and Africa.

(2) The similarity of the earthquake mechanisms for continental collision and oceanic subduction, and especially the very shallow dip of the inferred fault plane, which is uncommon for continental shortening, indicate that the process of brittle energy release is similar in the two regions and corresponds to a major active, or recent, boundary.

(3) The difference in the amplitude of the relative velocity deduced from seismic moment release and GPS displacement between continental collision and oceanic subduction can be explained in two ways.

Table 3. GPS displacement vectors.

Region	Sta	Lat (°N)	Lon (°E)	Khale		Europe		Africa		Mean	
				Az	Rate	Az	Rate	Az	Rate	Az	Rate
Collision	KARI	39.73	20.67	219	05	325	00	165	09	162±29	07±3
	AMAT	39.52	19.85	287	01	015	05	139	06		
	TERO	39.47	20.88	228	08	245	04	184	10		
	PARG	39.28	20.47	269	06	314	05	196	05		
	GAIO	39.20	20.20	327	03	006	07	127	04		
Lefkada	IKVL	38.78	20.65	209	13	208	09	186	17	187±01	18±2
	VASI	38.60	20.57	206	16	205	12	188	19		
Kefallinia	EXOG	38.45	20.63	217	19	219	15	199	21	198±09	19±2
	ASSO	38.37	20.55	221	15	227	11	199	17		
	SARA	38.37	20.73	207	18	207	14	191	21		
	KIAM	38.22	20.37	233	17	241	14	212	18		
	TSAR	38.17	20.68	212	18	214	14	195	21		
	LKTR	38.13	20.52	206	13	206	09	186	17		
Zakynthos	SKIN	37.93	20.70	223	20	227	16	206	22	212±08	28±6
	KSSI	37.72	20.98	217	26	219	22	204	28		
	LOGO	37.68	20.80	230	25	235	21	216	26		
	STRO	37.25	21.02	231	34	235	31	221	36		
Pelo	LAKA	38.23	21.97	200	23	198	19	188	28	205±08	34±5
	SNDO	38.02	21.58	221		223	29	210	35		
	CHLE	37.88	21.13	215	23	217	19	201	26		
	DOXA	37.70	21.93	217	34	218	31	207	38		
	ZAHA	37.48	21.65	221	36	223	33	211	39		
	AETO	37.25	21.83	221	37	223	34	212	40		
	XRIS	36.78	21.88	222	33	224	30	212	36		
	DION	38.08	23.93	218	32	218	29	207	36		
Akarnania	ATKO	38.50	21.12	205	23	204	19	192	27	198±09	26±6
	KRPN	38.90	21.80	230	23	233	19	212	24		
	MESS	38.37	21.12	205	30	204	26	194	33		
	VONI	38.92	20.85	215	17	216	13	195	20		

Downloaded from http://gji.oxfordjournals.org/ at Observatoire de la CÃ'te d'Azur - Geoazur on December 13, 2016

(a) There is a dynamic process that needs to be taken into account. For instance, if the continental collision is recent, the displacement should vary from collision to subduction, but not necessarily the stress release and therefore the level of seismicity. The idea of a recent continental collision is supported by the slight change in the azimuth (which varies from 27° to 36°) and values of GPS displacement (which varies from 1.4–3.1 cm yr^{-1}) going to the south of the Ionian islands compared with the constant azimuth of the earthquake slip vectors along the active boundary. This is also supported by the low-angle reverse faulting, usual for oceanic subduction but not for intracontinental shortening.

(b) The brittle seismic energy release is related only to part of the total deformation and depends on the type of deformation. To the north (continental collision) GPS displacements and seismic energy release lead to a similar rate of deformation, which means that most of the deformation is seismic. To the south (oceanic subduction) only a small part (about 35–40 per cent) of the deformation may be released as seismic energy. This was pointed out by Jackson & McKenzie (1988).

5 CONCLUSIONS

We presented in this paper the most reliable solutions for 32 earthquakes that occurred in the western Hellenic area. The technique that we used (body-wave modelling) allows a greater accuracy in the azimuth of the slip vector than the first-motion polarity method that was used in previous studies related to the same area.

The solutions clearly show that normal faulting dominates within the internal part of the Aegean area, from Albania to the southern Peloponnese. The trend of the *T*-axes is consistently N–S in central Greece from Thessaloniki to the Gulf of Corinth. It seems to be trending more NW–SE towards the active boundaries.

The mechanisms clearly show strike-slip motion associated with a transform zone along the Ionian islands. The azimuth of the slip vectors is consistent with the azimuth of the motion of the Ionian islands relative to Matera, but is slightly different from the strike of the main tectonic feature of Kefallinia and should create some reverse feature.

Reverse faulting is observed along the entire length of the active boundary and does not depend on the type of convergence (continental collision or oceanic subduction). There is a remarkable consistency in the trend and dip of the probable fault plane and the trend of the slip vector all along the boundary. The consistent pattern of reverse mechanisms all along the active boundary and of normal faulting inside the Aegean suggests that the mechanism responsible for the deformation is at a scale comparable to the Aegean itself. The inconsistency between the geodetic measurements on the one side and the earthquake mechanisms on the other suggests that the proportion of seismic energy release depends on the type of convergence (continental collision or oceanic subduction), or represents different states of the same process and therefore that western Hellenic geodynamics is in a transitional state.

ACKNOWLEDGMENTS

CB thanks the DRED of the French Ministère de l'Education Nationale for supporting his post-doctoral fellowship in Grenoble. X. LePichon pointed out that the reference frame of GPS displacements should be Africa and B. Chamot-Rooke kindly provided the vectors used in Table 3. We benefited from the constructive reviews of J. Jackson and C. Langston.

REFERENCES

Academy of Sciences, 1983. The earthquake of 1979 April 15 and the elimination of its consequences, *Report and papers on the Shkodra symposium,* Nentori Publishing House, Tirana, Albania.

Aki, K. & Richards, P.G., 1980. *Quantitative Seismology,* W.H. Freeman, San Francisco, CA.

Ambraseys, N.N., 1975. Studies in historical seismicity and tectonics, *Geodynamics Today,* Royal Society of London, 7–16.

Ambraseys, N. & Jackson, J., 1990. Seismicity and associated strain of Central Greece between 1890 and 1988, *Geophys. J. Int.,* **101,** 663–708.

Anderson, H.J. & Jackson, J.A., 1987. Active tectonics of the Adriatic region, *Geophys. J. R. astr. Soc.,* **91,** 937–983.

Argus, D.F., Gordon, R.G., DeMets, Ch. & Stein, S., 1989. Closure of the Africa-Eurasia-North America plate motion circuit and tectonics of the Gloria Fault, *J. geophys. Res.,* **94,** 5585–5602.

Armijo, R., Lyon-Caen, H. & Papanastassiou, D., 1992. East–west extension and Holocene normal-fault scarps in the Hellenic arc, *Geology,* **20,** 491–494.

Armijo, R., Meyer, B., King, G.C.P., Rigo, A. & Papanastassiou, D., 1996. Quaternary evolution of the Corinth Rift and its implications for the late Cenozoic evolution of the Aegean, *Geophys. J. Int.,* **126,** 11–53.

Barker, J.S. & Langston, C.A., 1981. Inversion of teleseismic body waves for the moment tensor of the 1978 Thessaloniki Greece earthquake, *Bull. seism. Soc. Am.,* **71,** 1423–1444.

Bernard, P. *et al.* 1997. A low angle normal fault earthquake: the Ms = 6.2, June, 1995 Aigion earthquake (Greece), *J. Seism.,* in press.

Bezzeghoud, M., Deschamps, A. & Madariaga, R., 1986. Broad-band modelling of the Corinth, Greece earthquakes of February and March 1981, *Ann. Geophys.,* **4,** 295–304.

Boore, D.M., Sims, J.D., Kanamori, H. & Harding, S., 1981. The Montenegro, Yugoslavia earthquake of April 15, 1979: source orientation and strength, *Phys. Earth planet. Inter.,* **27,** 133–142.

Briole, P., Deschamps, A., Lyon-Caen, H., Papazissi, K. & Martinod, J., 1993. The Itea (Ms ≈ 5.9) earthquake of November 18, 1992. Characteristics of the main shock inferred from body wave and ground displacement analysis, *2nd Congress of the Hellenic Geophysical Union, Florina,* 5–7 May 1993, Greece.

Brooks, M., Clews, J.E., Melis, N.S. & Underhill, J.R., 1988. Structural development of Neogene basins in western Greece, *Basin Res.,* **1,** 129–138.

Channell, J.E.T., D'Argenio, B. & Horvath, F., 1979. Adria, the African promontory, in *Mesozoic Mediterranean Paleogeography, Earth Sci. Rev.,* **15,** 213–292.

Console, R. & Favalli, P., 1981. Study of the Montenegro earthquake sequence (March-July 1979), *Bull. seism. Soc. Am.,* **71,** 1233–1248.

Cushing, M., 1985. Evolution structurale de la marge nord-ouest hellénique dans l'île de Levkas et ses environs (grèce nord-occidentale), *Thèse de 3 ème cycle,* Université de Paris XI.

Dziewonski, A., Friedman, A. & Woodhouse, J.H., 1983. Centroid-moment tensor solutions for January-March, 1983, *Phys. Earth planet. Inter.,* **33,** 71–75.

Fitch, T.J. & Muirhead, K.J., 1974. Depths to larger earthquakes associated with crustal loading, *Geophys. J. R. astr. Soc.,* **37,** 285–296.

Frederich, J., McCaffrey, R. & Denham, D., 1988. Source parameters of seven large Australian earthquakes determined by body waveform inversion, *Geophys. J.,* **95,** 1–13.

Giardini, D., Dziewonski, A.M., Woodhouse, J.H. & Boschi, E., 1984. Systematic analysis of the seismicity of the Mediterranean region

Downloaded from http://gji.oxfordjournals.org/ at Observatoire de la CÃ'te d'Azur - Geoazur on December 13, 2016

using centroid-moment tensor method, *Bull. Geofis. teor. appl.*, **XXVI,** 121–142.

Hatzfeld, D., Christodoulou, A.A., Scordilis, E.M., Panagiotopoulos, D.G. & Hatzidimitriou, P.M., 1987. A microearthquake study of the Mygdonian graben (Northern Greece), *Earth planet. Sci. Lett.*, **81,** 379–396.

Hatzfeld, D. *et al.* 1989. The Hellenic subduction beneath the Peloponnesus: first results of a microearthquake study, *Earth planet. Sci. Lett.*, **93,** 283–291.

Hatzfeld, D., Pedotti, G., Hatzidimitriou, P. & Makropoulos, K, 1990. The strain pattern in the western Hellenic arc deduced from a microearthquake survey, *Geophys. J. Int.*, **101,** 181–202.

Hatzfeld, D., Besnard, M., Makropoulos, K. & Hatzidimitriou, P., 1993. Microearthquake seismicity and fault plane solutions in the southern Aegean and its tectonic implications, *Geophys. J. Int.*, **115,** 799–818.

Hatzfeld, D., Kassaras, I., Panagiotopoulos, D., Amorese, D., Makropoulos, K., Karakaisis, G. & Coutant, O., 1995. Microseismicity and strain pattern in Northwestern Greece, *Tectonics,* **14,** 773–785.

Hatzfeld, D., Martinod, J., Bastet, G. & Gautier, P., 1997. An analog model for the Aegean to describe the contribution of gravitational potential energy, *J. geophys. Res.*, **102,** 649–659.

Hatzfeld, D. *et al.* 1996. The Galaxidi earthquake sequence of November 18, 1992: a possible geometrical barrier within the normal fault system of the Gulf of Corinth (Greece), *Bull. seism. Soc. Am.*, **86,** 1987–1991.

Hatzfeld, D. et al. 1997. The Kozani-Grevena earthquake of May 13, 1997. A seismological study. *Bull. seism. Soc. Am.*, **87,** 463–473.

Ioannidou, E., 1989. Characteristics parameters of seismic source by the method of body wave inversion: Greece and surrounding area, *PhD thesis,* University of Athens, Greece.

Jackson, J.A., 1994. The Aegean deformation, *Ann. Rev. Geophys.*, **22,** 239–272.

Jackson, J.A., Gagnepain, J., Houseman, G., King, G.C.P., Papadimitriou, P., Soufleris, C. & Virieux, J., 1982. Seismicity, normal faulting, and the geomorphological development of the Gulf of Corinth (Greece): the Corinth earthquakes of February & March 1981, *Earth planet Sci. Lett.*, **57,** 377–397.

Jackson, J.A. & McKenzie, D.P., 1984. Active tectonics of the Alpine-Himalayan belt between western Turkey and Pakistan, *Geophys. J. R. astr. Soc.*, **77,** 185–264.

Jackson, J.A. & McKenzie, D., 1988. The relationship between plate motions and seismic moment tensors, and the rates of active deformation in the Mediterranean and the Middle East, *Geophys. J.*, **93,** 45–73.

Jackson, J.A. & White, N.J., 1989. Normal faulting in the upper continental crust: observations from regions of active extension, *J. struct. Geol.*, **11,** 15–36.

Kahle, H-G, Müller, M.V., Mueller, S., Veis, G., 1993. The Kephalonia transform fault and the rotation of the Apulian plateform: evidence from satellite geodesy, *Geophys. Res. Lett.*, **20,** 651–654.

Kahle, H-G. *et al.*, 1995. The strain field in NW Greece and the Ionian islands: results inferred from GPS measurements, *Tectonophysics,* **249,** 41–52.

Kanamori, H. & Given, J.W., 1981. Use of long-period surface waves for rapid determination of earthquake-source parameters, *Phys. Earth planet. Inter.*, **27,** 8–31.

King, G.C.P. *et al.*, 1985. The evolution of the Gulf of Corinth (Greece): an aftershock study of the 1981 earthquakes, *Geophys. J. R. astr. Soc.*, **80,** 677–693.

Kiratzi, A.A. & Langston, Ch., A., 1989. Estimation of earthquake source parameters of the May 4, 1972 event of the Hellenic arc by the inversion of waveform data, *Phys. Earth planet. Inter.*, **57,** 225–232.

Kiratzi, A.A. & Langston, Ch. A., 199. Moment tensor inversion of the 1983 January 17 Kefallinia event of Ionian islands (Greece), *Geophys. J. Int.*, **105,** 529–535.

Kissel, C. & Laj, C., 1988. The tertiary geodynamical evolution of the Aegean arc; a palaeomagnetic reconstruction, *Tectonophysics,* **146,** 183–201.

Le Pichon, X. & Angelier, J., 1979. The Hellenic arc and trench system: a key to the neotectonic evolution of the Eastern Mediterranean region, *Tectonophysics,* **60,** 1–42.

Le Pichon, X., Chamot-Rooke, N., Lallemant, S., Noomen, R. & Veis, G., 1995. Geodetic determination of the kinematics of Central Greece with respect to Europe: Implications for Eastern Mediterranean Tectonics, *J. geophys. Res.*, **100,** 12 675–12 690.

Liotier, Y., 1989. Modelisation des ondes de volume des séismes de l'arc égéen, *DEA de l'Université Joseph Fourier,* Grenoble, France.

Lyon-Caen, H. *et al.*, 1988. The 1986 Kalamata (South Peloponnesus) earthquake: detailed study of a normal fault, evidences for east–west extension in the Hellenic Arc, *J. geophys. Res.*, **93,** 14 967–15 000.

McCaffrey, R. & Nabelek, J., 1987. Earthquakes, gravity, and the origin of the Bali basin: an example of a nascent continental fold and thrust belt, *J. geophys. Res.*, **92,** 441–460.

McCaffrey, R., Abers G. & Zwick, A., 1991. Inversion of teleseismic body waves, in *Digital Seismogram Analysis and Waveform Inversion,* ed. Lee, W., IASPEI Software Library, Vol. 3, Menlo Park, USA.

McKenzie, D.P., 1972. Active tectonics of the Mediterranean region, *Geophys. J. R. astr. Soc.*, **30,** 109–185.

McKenzie, D.P., 1978. Active tectonics of the Alpine-Himalayan belt: the Aegean Sea and surrounding regions, *Geophys. J. R. astr. Soc.*, **55,** 217–254.

Mercier, J.L., Mouyaris, N., Simeakis, C., Roundoyanni, T. & Angelidhis, C., 1979. Intraplate deformation: a quantitative study of the faults activated by the 1978 Thessaloniki earthquakes, *Nature,* **278,** 45–48.

Mercier, J.L., Carey-Gailhardis, E., Mouyaris, N., Simeakis, C., Roudoyanni, T. & Angelidhis, C., 1983. Structural analysis of recent and active faults and regional state in the epicentral area of the 1978 Thessaloniki earthquake (Northern Greece), *Tectonics,* **2,** 577–600.

Mercier, J.-L., Sorel, D. & Simeakis, K., 1987. Changes in the state of stress in the overriding plate of a subduction zone, the Aegean arc from the Pliocene to the Present, *Ann. Tectonicae,* **1,** 20–39.

Molnar, P. & Lyon-Caen, H., 1989. Fault plane solutions of earthquakes and active tectonics of the Tibetan Plateau and its margins, *Geophys. J. Int.*, **99,** 123–153.

Nabelek, J.L., 1984. Determination of earthquake source parameters from inversion of body waves, *PhD thesis,* Massachusetts Institute of Technology, Cambridge, MA.

Nelson, M., McCaffrey, R. & Molnar, P., 1987. Source parameters for 11 earthquakes in the Tien Shan, Central Asia, determined by P and SH waveform inversion, *J. geophys. Res.*, **92,** 12 629–12 648.

Noomen, R., Ambrosius, D.C., Kuiper, D.C., Mets, G.J., Springer, T. & Wakker, K.F., 1994. Rigid block deformations in Southeast Europe, *First Turkish Symposium on Deformations,* Istanbul, 5–9 September, pp. 713–728, TMMOB-HKMO, Chambers of Survey & Engineers, Ankara, Turkey.

Panagiotopoulos, D.G. & Papazachos, B.C., 1985. Travel times of *Pn* waves in the Aegean and surrounding area, *Geophys. J. R. astr. Soc.*, **80,** 165–176.

Papadimitriou, E.E., 1993. Focal mechanisms along the convex side of the Hellenic arc, *Boll. Geofis. Teorica Appl.*, **140,** 401–426.

Papadimitriou, P., 1988. Etude de la structure du manteau supérieur de l'Europe et modélisation des ondes de volume engendrées par les séismes égéens, *Thèse,* l'Université de Paris VII.

Papadimitriou, E. & Papazachos, B., 1985, Evidence for premonitory patterns in the Ionian islands (Greece), *Earthq. Predict. Res.*, **3,** 95–103.

Papazachos, B.C., Mountrakis, D., Psilovicos, A. & Levantakis, G., 1979. Surface fault traces and fault plane solutions of the May-June 1978 shocks in the Thessaloniki area, North Greece, *Tectonophysics,* **53,** 171–183.

Papazachos, B. *et al.*, 1982. Atlas of Isoseismal maps for earthquakes

Downloaded from http://gji.oxfordjournals.org/ at Observatoire de la CÃ´te d'Azur - Geoazur on December 13, 2016

in Greece, 1902–1981, *Publ. 4,* Geophysics Laboratory, University of Thessaloniki, Greece.

Papazachos, B.C., Kiratzi, A.A., Karacostas, B., Panagiotopoulos, D., Scordilis, E. & Mountrakis, D.M., 1988. Surface fault traces, fault plane solution and spatial distribution of the aftershocks of September 13, 1986 earthquake of Kalamata (Southern Greece), *Pure appl. Geophys.,* **126,** 55–68.

Papazachos, B. & Papazachou, K., 1989. *Earthquakes in Greece,* Ekdoseis Ziti, Thessaloniki.

Papazachos, B., Kiratzi, A. & Papadimitriou, E., 1991. Regional focal mechanisms for earthquakes in the Aegean area, *Pure appl. Geophys.,* **136,** 405–420.

Papazachos, C.B. & Kiratzi, A.A., 1996. A detailed study of the active crustal deformation in the Aegean and surrounding area, *Tectonophysics,* **253,** 129–153.

Philip, H., 1983. La tectonique actuelle et récente dans le domaine méditerranéens bordures, ses relations avec la sismicité, *Thèse,* Université des Sciences et Techniques du Languedoc, Montpellier, France.

Rigo, A., Lyon-Caen, H., Armijo, R., Deschamps, A., Hatzfeld, D., Makropoulos, K., Papadimitriou, P. & Kassaras, I., 1996. A micro-seismic study in the western part of the Gulf of Corinth (Greece): implications for large-scale normal faulting mechanisms, *Geophys. J. Int.,* **126,** 663–688.

Scordilis, E.M., Karakaisis, G.F., Karacostas, B.G., Panagiotopoulos, D.G., Comninakis, P.E. & Papazachos, B.C., 1985. Evidence for transform faulting in the Ionian Sea: The Cephalonia Islands earthquake sequence of 1983, *Pure appl. Geophys.,* **123,** 388–397.

Sorel, D., 1989. L'évolution structurale de la Grèce nord-occidentale depuis le Miocène, dans le cadre géodynamique de l'arc égéen, *Thèse de Doctorat d'Etat,* Université de Paris-Sud.

Soufleris, C. & Stewart, G.S., 1981. A source study of the Thessaloniki (Northern Greece) 1978 earthquake sequence, *Geophys. J. R. astr. Soc.,* **67,** 343–358.

Speranza, F., Islami, I., Kissel, C. & Hyseni, A., 1995. Palaeomagnetic evidence for Cenozoic clockwise rotation of the external Albanides, *Earth planet. Sci. Lett.,* **129,** 121–134.

Stein, S., Wiens, D.A. & Fujita, K., 1982. The 1966 Kremasta reservoir earthquake sequence, *Earth planet. Sci. Lett.,* **59,** 49–60.

Suarez, G., Molnar, P. & Burchfield, B.C., 1983. Seismicity, fault plane solutions, depth of faulting, and active tectonics of the central Andes, *J. geophys. Res.,* **88,** 10 403–10 428.

Sulstarova, E., 1980. The focal mechanism of the April 15, 1979, earthquake sequence, *Proc. 17th Assembly Europ. seism. Com.,* Budapest.

Sulstarova, E. & Kociaj, S., 1980. The Dibra (Albania) earthquake of November 30, 1967, *Tectonophysics,* **67,** 333–343.

Tagari, D., 1993. Etude neotectonique et sismotectonique des Albanides: analyse des deformations et Géodynamique du Langhien à l'actuel, *Thèse,* l'Université de Paris XI-Orsay.

Taymaz, T., Jackson, J.A. & McKenzie, D., 1991. Active tectonics of the north and central Aegean Sea, *Geophys. J. Int.,* **106,** 433–490.

Taymaz, T., Jackson, J.A. & Westaway, R., 1990. Earthquake mechanisms in the Hellenic Trench near Crete, *Geophys. J. Int.,* **102,** 695–732.

Underhill, J.R., 1989. Late Cenozoic deformation of the Hellenide foreland, western Greece, *Geol. Soc. Am. Bull.,* **101,** 613–634.

Ward, S.N., 1994. Constraints on the seismotectonics of the central Mediterranean from Very Long Baseline Interferometry, *Geophys. J. Int.,* **117,** 441–452.

Waters, D.W., 1993. The tectonic evolution of Epirus, N.W. Greece, *PhD thesis,* University of Cambridge.

Downloaded from http://gji.oxfordjournals.org/ at Observatoire de la CÃ'te d'Azur - Geoazur on December 13, 2016

APPENDIX A: OBSERVED AND SYNTHETIC SEISMOGRAMS

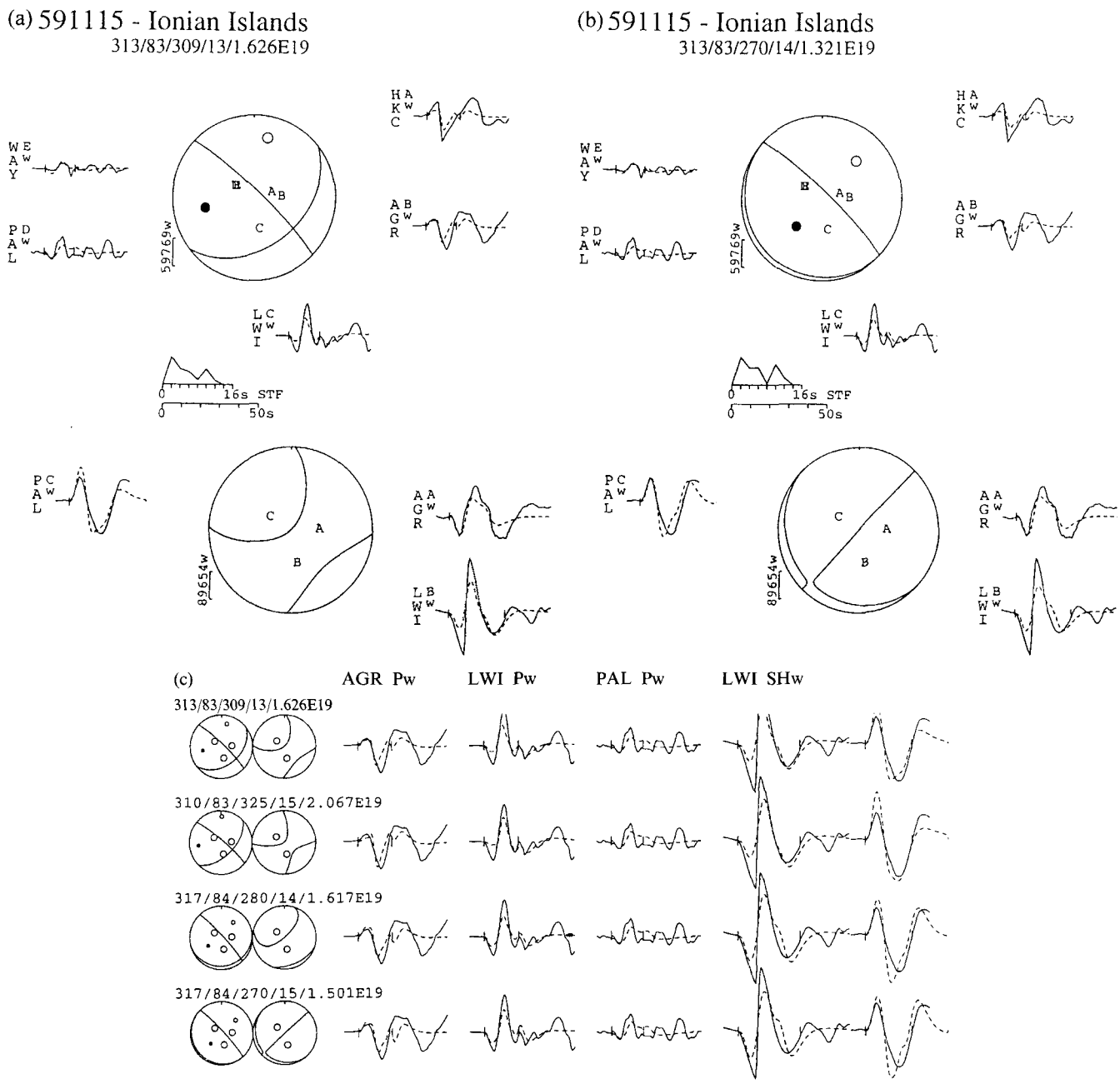

Figure A1. (a) This (and subsequent figures of this type) shows the radiation pattern and waveforms for the earthquake models presented in this study. Here the minimum-misfit solution for the 1959 November 15 event is shown. The header is the year–month–day and identification of the earthquake. The five numbers below this are the strike/dip/rake/centroid depth/seismic moment in N m for the model. The upper plot shows the *P*-wave radiation pattern and waveforms, the lower plot is for *SH* waves. The location of the station is reported on the focal sphere (lower hemisphere) and arranged clockwise. The *P*-axis is a solid dot, the *T*-axis an open dot. Surrounding the focal sphere, recorded waveforms are shown as continuous lines and computed synthetics as dashed lines. The waveform amplitudes have been normalized to that of an instrument with a gain of 3000 at a distance of 40°. The duration of the window used for the inversion is shown by vertical bars on the seismograms. To the left of each waveform the three-letter station code is written together, with a letter which identifies the position of the station on the focal sphere. 'w' indicates that the instrument is a WWSSN long-period seismometer. Left of the *P* focal sphere, a vertical bar indicates the scale of the seismogram in μm. Beneath the *P*-waveform plot, the source time function is shown and beneath this is the timescale for the seismogram. For each event, the first plot is always the minimum-misfit solution for which all the parameters were left free. (b) the second plot (when present) is our preferred solution in which one of the parameters (generally the strike of the fault plane) is fixed because of additional information. (b) Our preferred solution for the event of 1959 November 15. In this case the rake has been fixed at 270° (−90°) to give a pure dip-slip thrust mechanism similar to mechanisms of nearby events (#2, 9, 12). (c) In this (and subsequent diagrams of this type) each row shows a selection of observed waveforms and synthetics returned in the inversion procedure. The top row always shows the minimum-misfit solution. Subsequent rows show the fits from

Downloaded from http://gji.oxfordjournals.org/ at Observatoire de la CÃ'te d'Azur - Geoazur on December 13, 2016

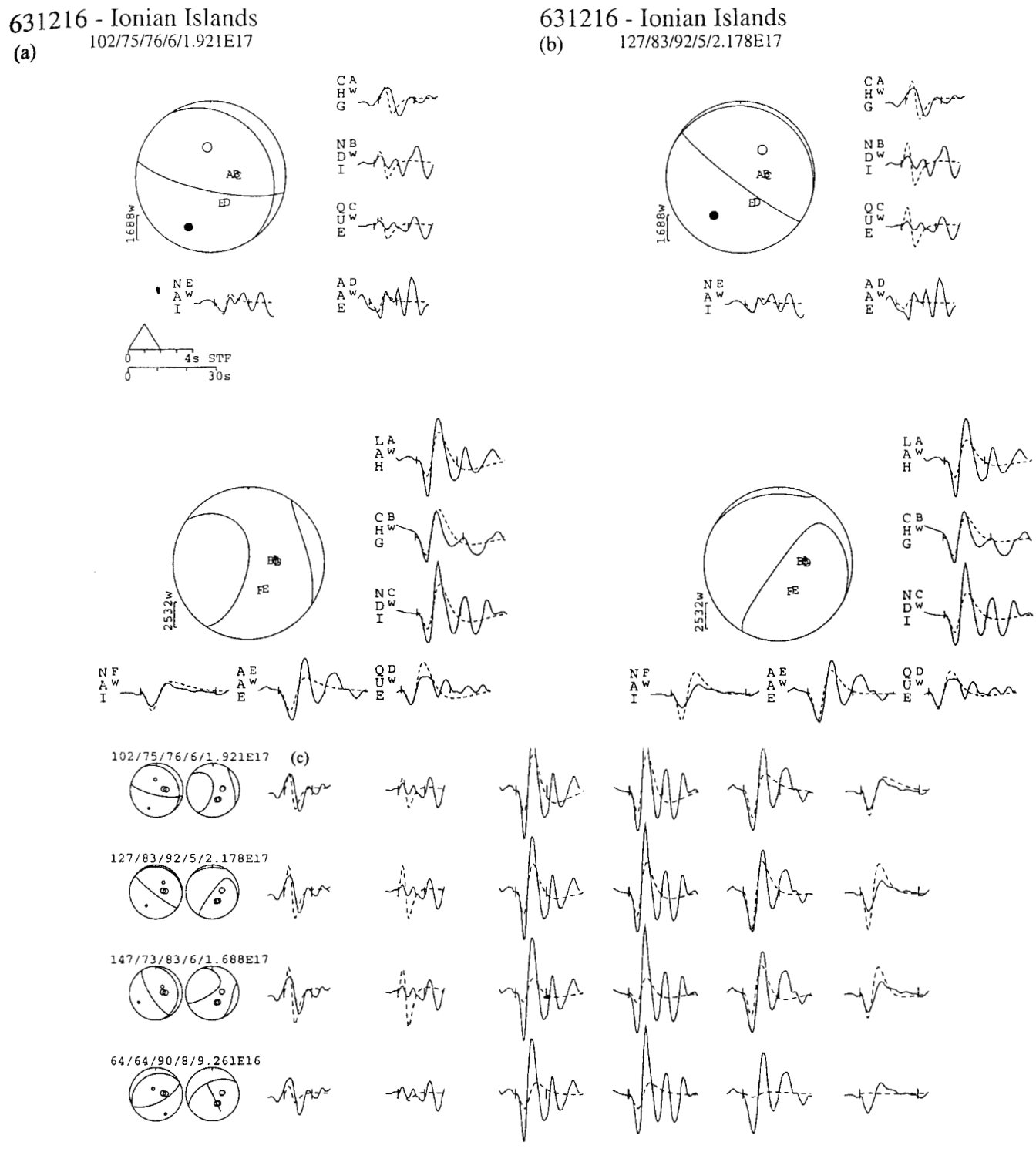

Figure A2. (a) Minimum-misfit solution for the earthquake of 1963 December 16, event 2. (b) The preferred solution for the earthquake of 1963 December 16. The strike of the fault plane is fixed parallel to the local bathymetry. (c) A comparison of different source orientations for the event of 1963 December 16. The display convention is the same as used in Fig. A1. The top line shows the minimum-misfit solution, Line 2 shows our preferred solution. Line 3 is computed with the strike fixed at 147°. Line 4 is the solution of Anderson & Jackson (1987) based on first-motion readings.

Caption A1. (*Continued*). models obtained in other studies or where one parameter has been fixed in the inversion. Each line starts with the *P* and *SH* focal spheres, above which are the values of the different parameters in the order strike/dip/rake/depth/moment. The stations are identified at the top of each column, together with the type of waveform, *P* or *SH*. This diagram shows a series of possible mechanisms for the event of 1959 November 15. The top line shows the minimum-misfit solution. Lines 2, 3 and 4 show the effect of fixing the NE–SW-striking nodal plane at different dip values than those in the minimum-misfit solution. Note how this plane is poorly constrained by the available data.

Downloaded from http://gji.oxfordjournals.org/ at Observatoire de la CÃ'te d'Azur - Geoazur on December 13, 2016

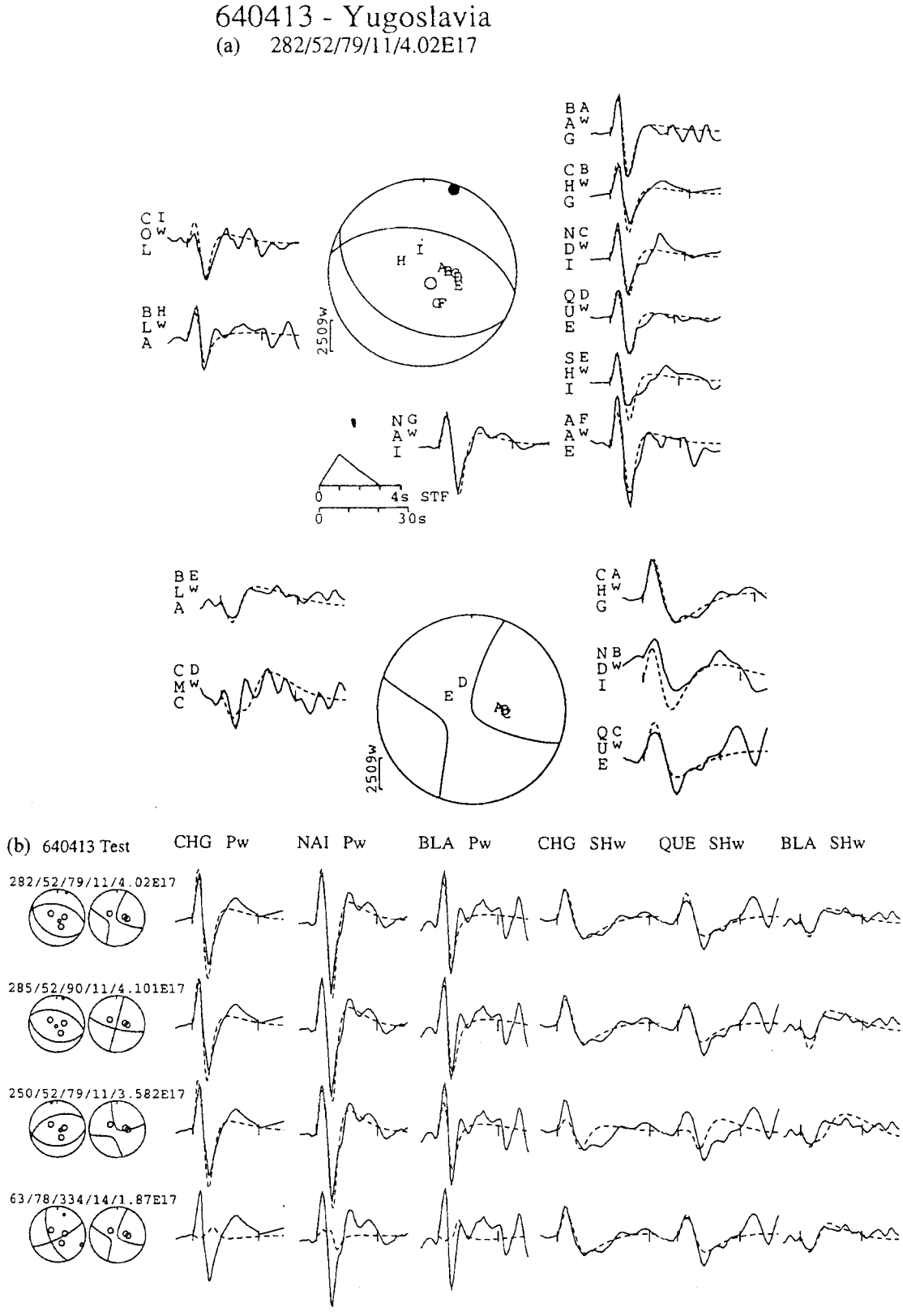

Figure A3. (a) Minimum-misfit solution for the earthquake of 1964 April 13, event 3. (b) A comparison of different source orientations for the 1964 April 13 event. Line 1 shows the minimum-misfit solution. Line 2 shows a mechanism with the rake constrained to give a pure dip-slip solution. Line 3 is a mechanism of the same orientation as that proposed by McKenzie (1972). Line 4 is a strike-slip mechanism similar to that found by Anderson & Jackson (1987) for other events in close proximity to this event.

Downloaded from http://gji.oxfordjournals.org/ at Observatoire de la CÃ´te d'Azur - Geoazur on December 13, 2016

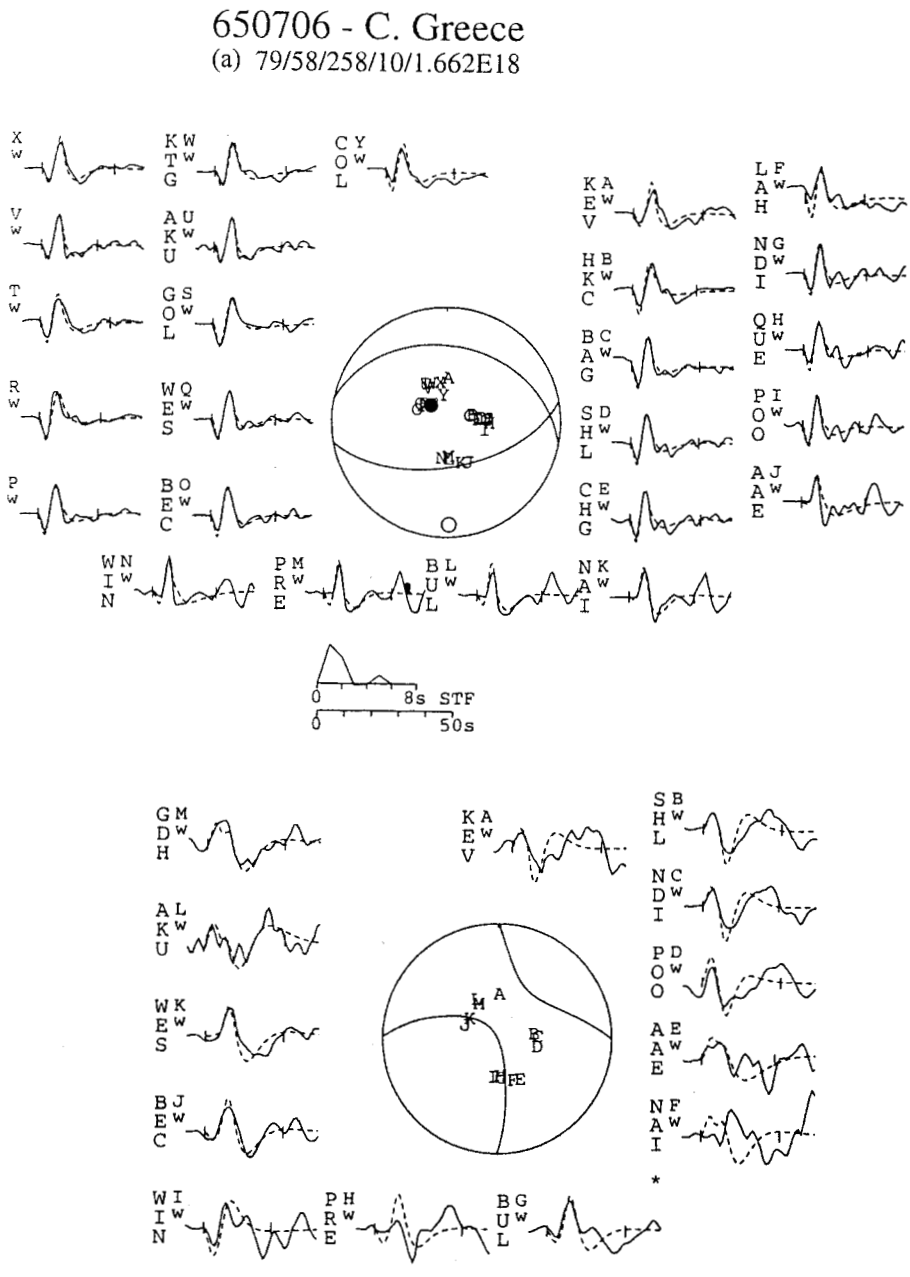

Figure A4. (a) Minimum-misfit solution for the event of 1965 July 6. (b) Strike test for event 4. This diagram (together with c, d and e) shows the procedure adopted for determining the uncertainties in different parameters, as outlined in Section 3. In each diagram, the minimum-misfit solution is the top line and other lines show the effect of fixing the parameter under test (marked with a black box in the top line) and allowing the other parameters to vary freely. The source time function for each of the mechanisms is also shown. Where the resulting match between the observed and synthetic waveforms is worse than in the minimum-misfit case, the waveform is marked with a vertical bar. If the match seems to be improved, the waveform is matched with a star. (c) Dip test for event 4. (d) Rake test for event 4. (e) Depth test for event 4.

Downloaded from http://gji.oxfordjournals.org/ at Observatoire de la CÃ´te d'Azur - Geoazur on December 13, 2016

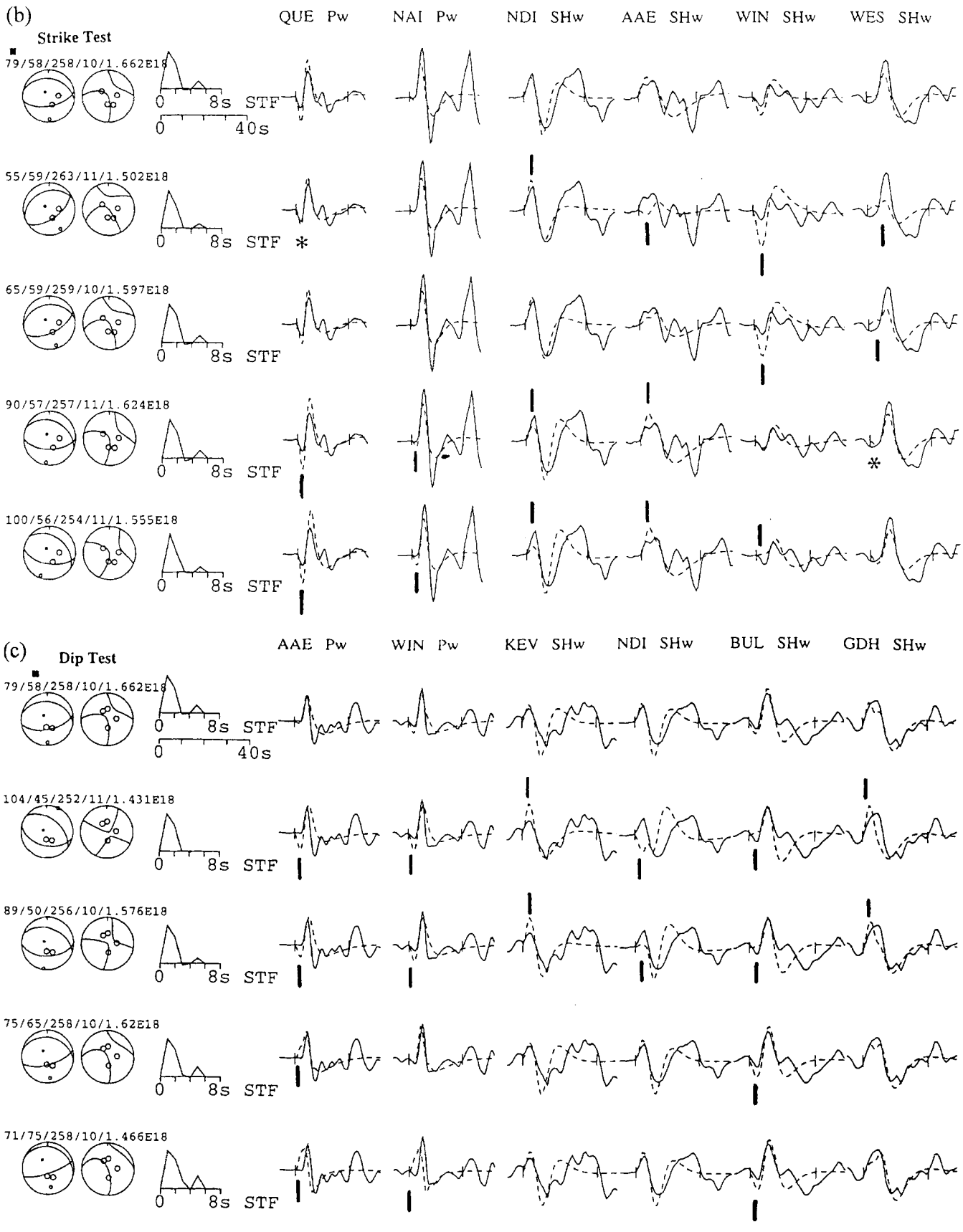

Figure A4. (*Continued.*)

Downloaded from http://gji.oxfordjournals.org/ at Observatoire de la CÃ´te d'Azur - Geoazur on December 13, 2016

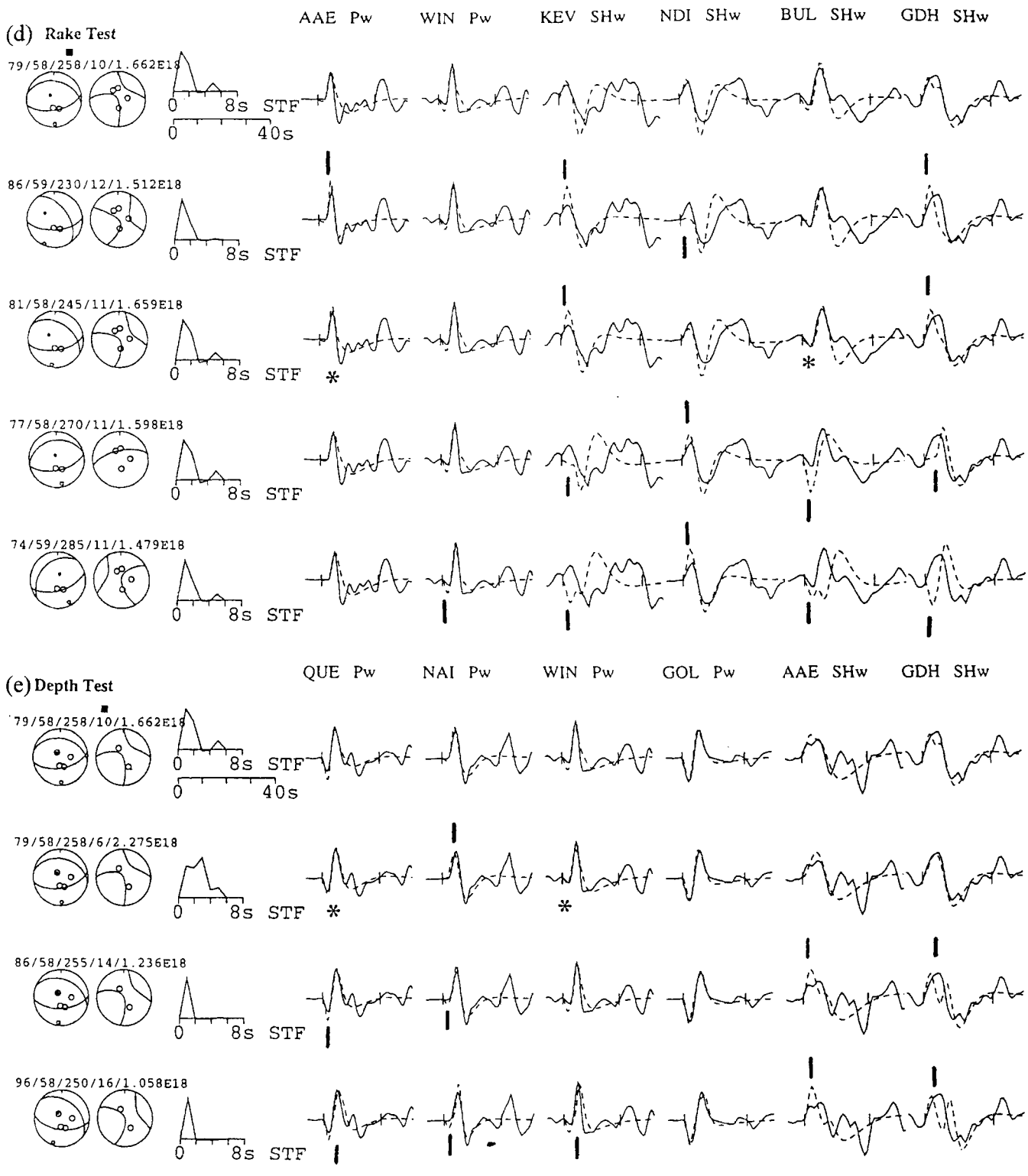

Figure A4. (*Continued.*)

Downloaded from http://gji.oxfordjournals.org/ at Observatoire de la CÃ´te d'Azur - Geoazur on December 13, 2016

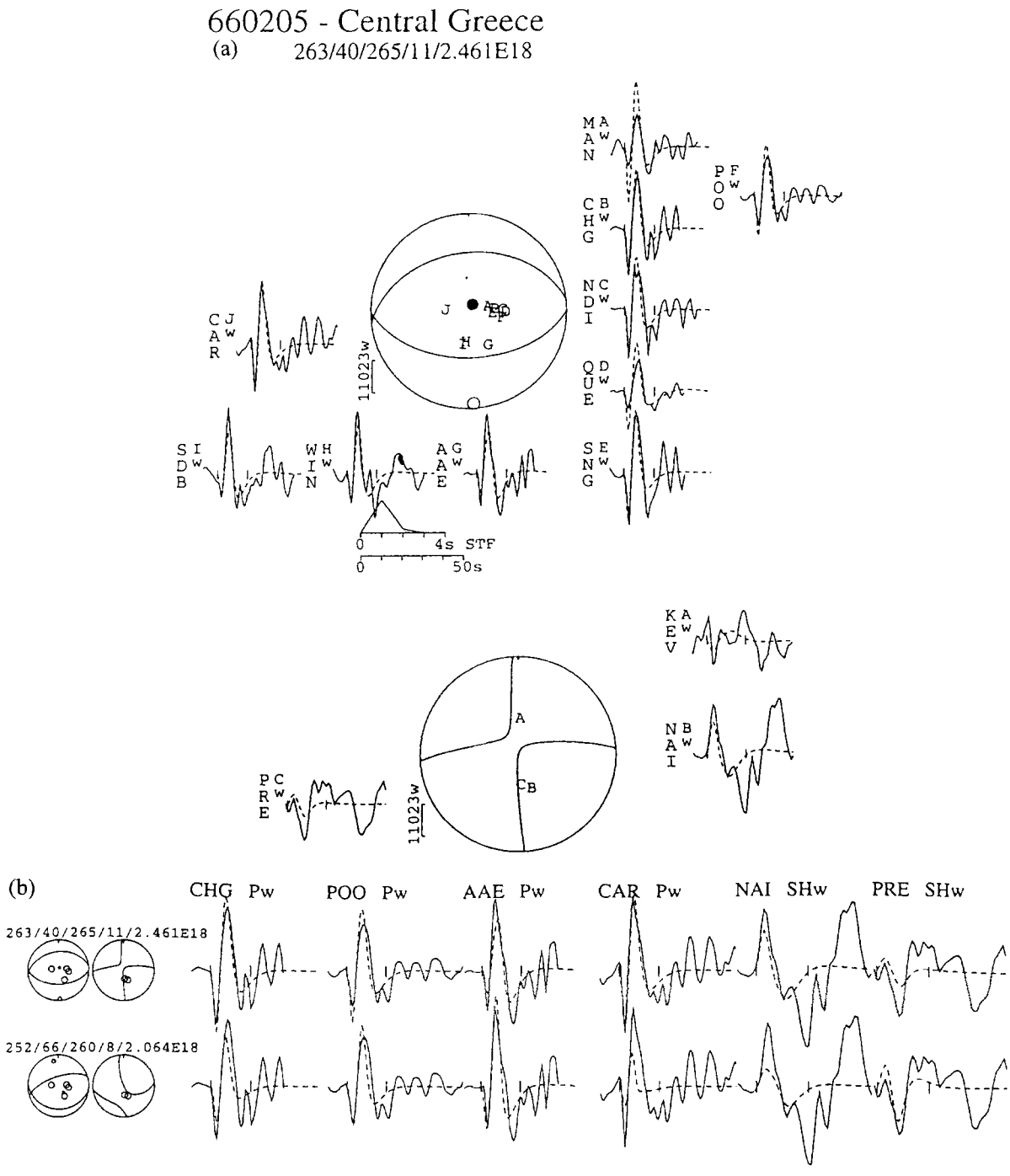

Figure A5. (a) Minimum-misfit solution for the earthquake of 1966 February 5. (b) A comparison of different source orientations for the event of 1966 February 5. The top line shows the minimum-misfit solution. Line 2 shows the mechanism proposed by Anderson & Jackson (1987) based on first-motion readings.

Downloaded from http://gji.oxfordjournals.org/ at Observatoire de la CÃ'te d'Azur - Geoazur on December 13, 2016

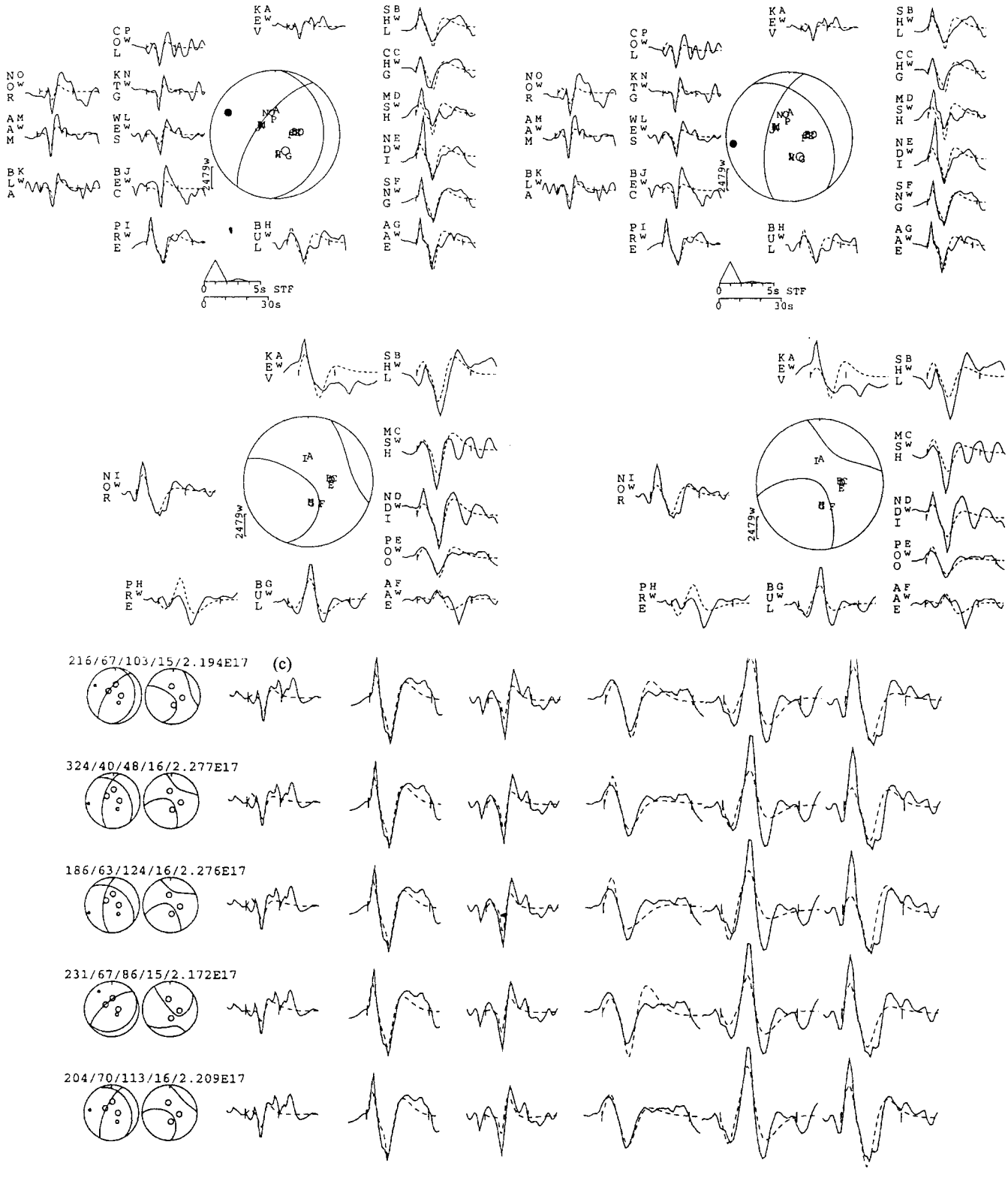

Figure A6. (a) Minimum-misfit solution for the earthquake of 1966 October 29. (b) The preferred solution for the mechanism of 1966 October 29. The strike of the fault plane is closer to the Katouna valley. (c) A comparison of different source orientations for the 1966 October 29 event. Lines 1 and 2 show our minimum-misfit and preferred solutions, respectively. Lines 3 and 4 show the effect of fixing the strike at values which differ from the minimum-misfit solution by $-30°$ and $+15°$. Line 5 shows the fits for the mechanism proposed by Anderson & Jackson (1987).

Downloaded from http://gji.oxfordjournals.org/ at Observatoire de la CÃ'te d'Azur - Geoazur on December 13, 2016

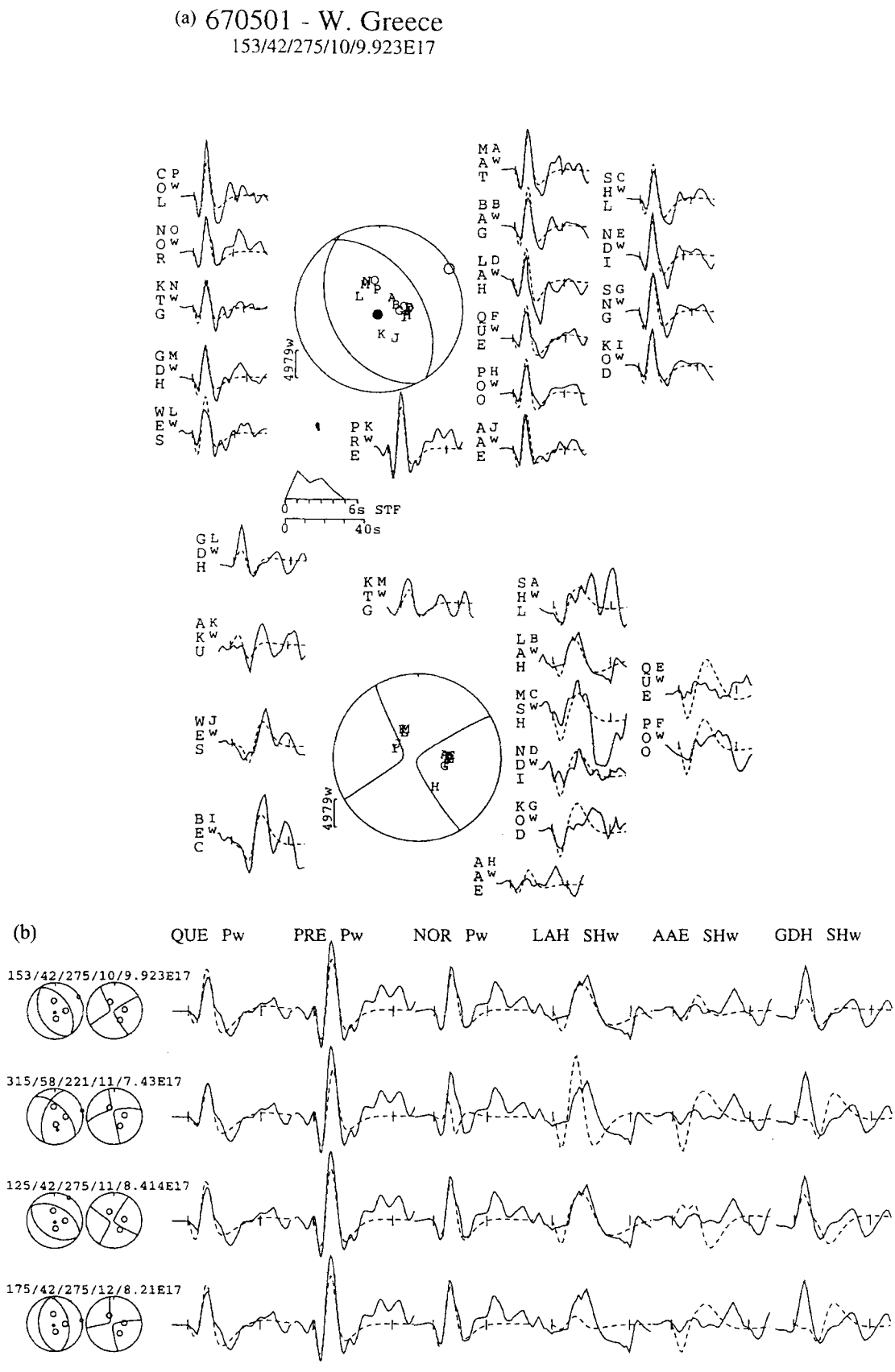

Figure A7. (a) Minimum-misfit solution for the earthquake of 1967 May 1. (b) A comparison of different source mechanisms for the event of 1967 May 1. Line 1 shows the minimum-misfit solution. Line 2 shows the well-constrained mechanism based on first-motion polarities proposed by Anderson & Jackson (1987). Lines 3 and 4 show the effect of fixing the strike at values which differ significantly (−28 and +22, respectively) from the minimum-misfit solution value.

Downloaded from http://gji.oxfordjournals.org/ at Observatoire de la CÃ'te d'Azur - Geoazur on December 13, 2016

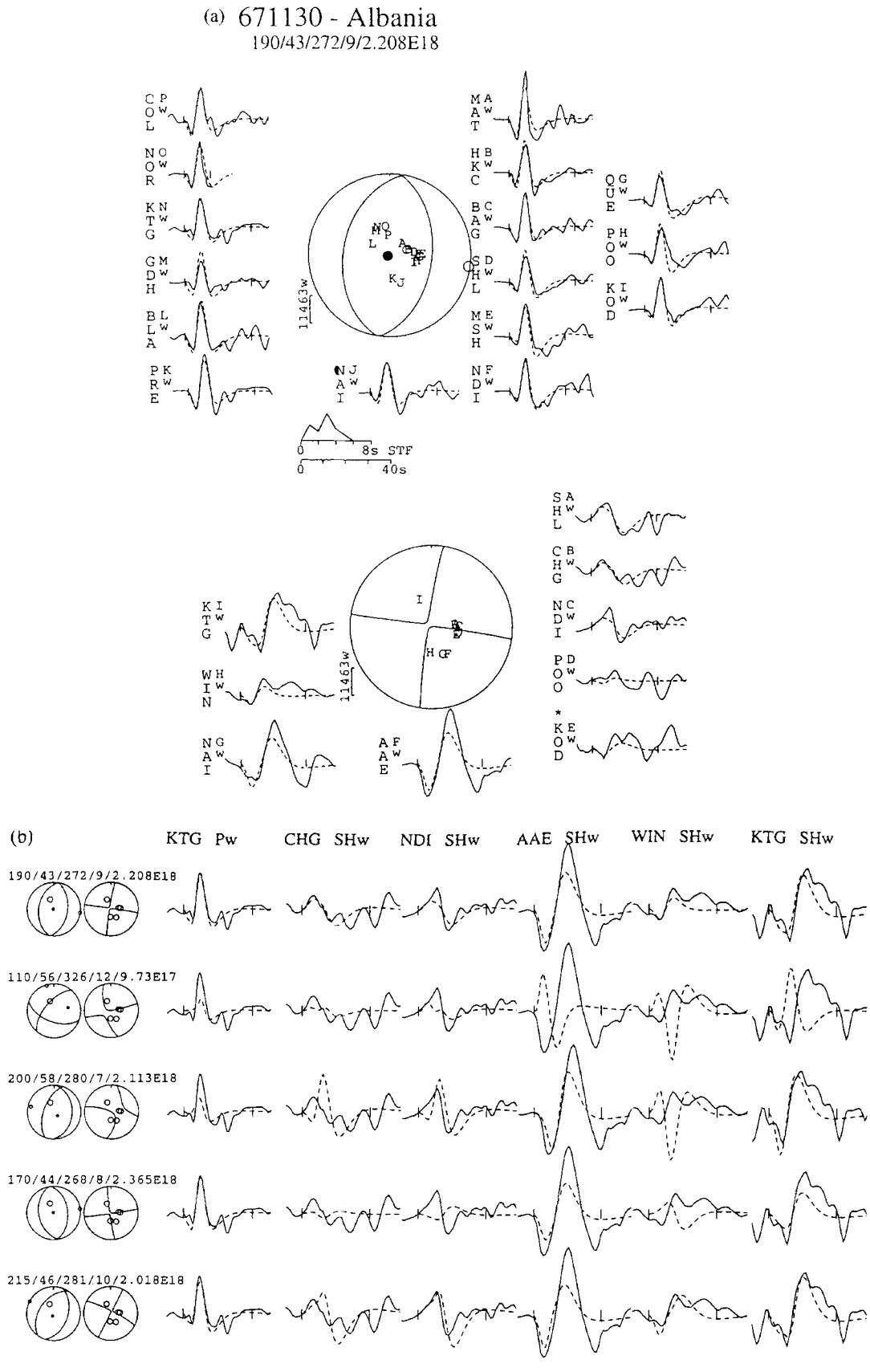

Figure A8. (a) Minimum-misfit solution for the earthquake of 1967 November 30. (b) A comparison of different source mechanisms for the event of 1967 November 30. The top line shows the minimum-misfit solution. Lines 2 and 3 show the mechanisms proposed by Sulstarova & Kociaj (1980) and Anderson & Jackson (1987), respectively. Lines 4 and 5 show the mechanism obtained when the strike is fixed at values of −20 and +25 relative to the minimum-misfit solution and the other parameters are allowed to vary freely.

Downloaded from http://gji.oxfordjournals.org/ at Observatoire de la CÃ´te d'Azur - Geoazur on December 13, 2016

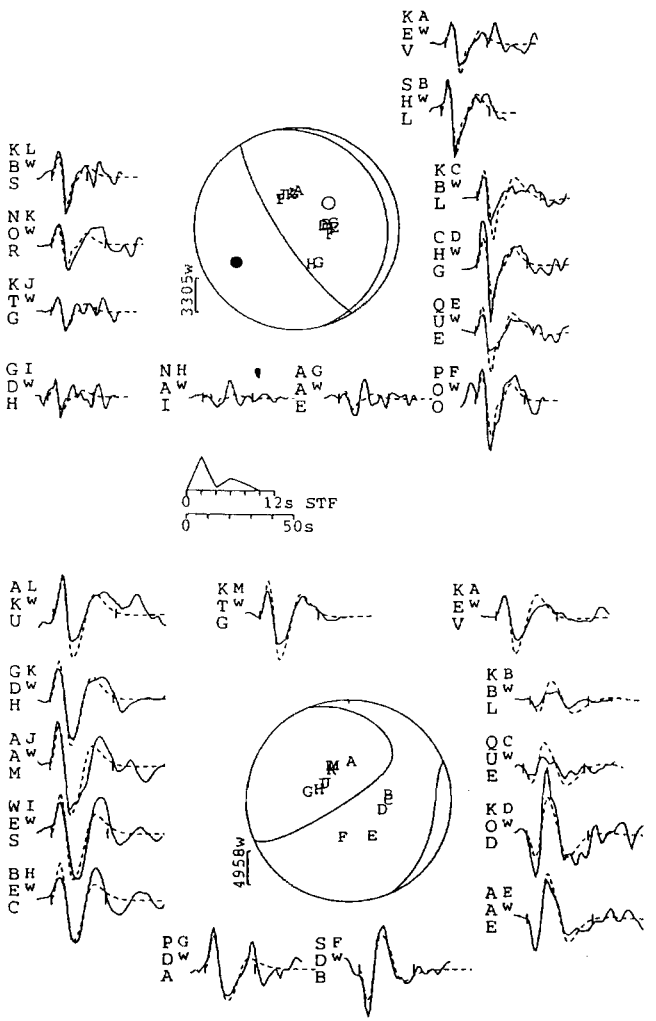

Figure A9. Minimum-misfit solution for the earthquake of 1969 July 8.

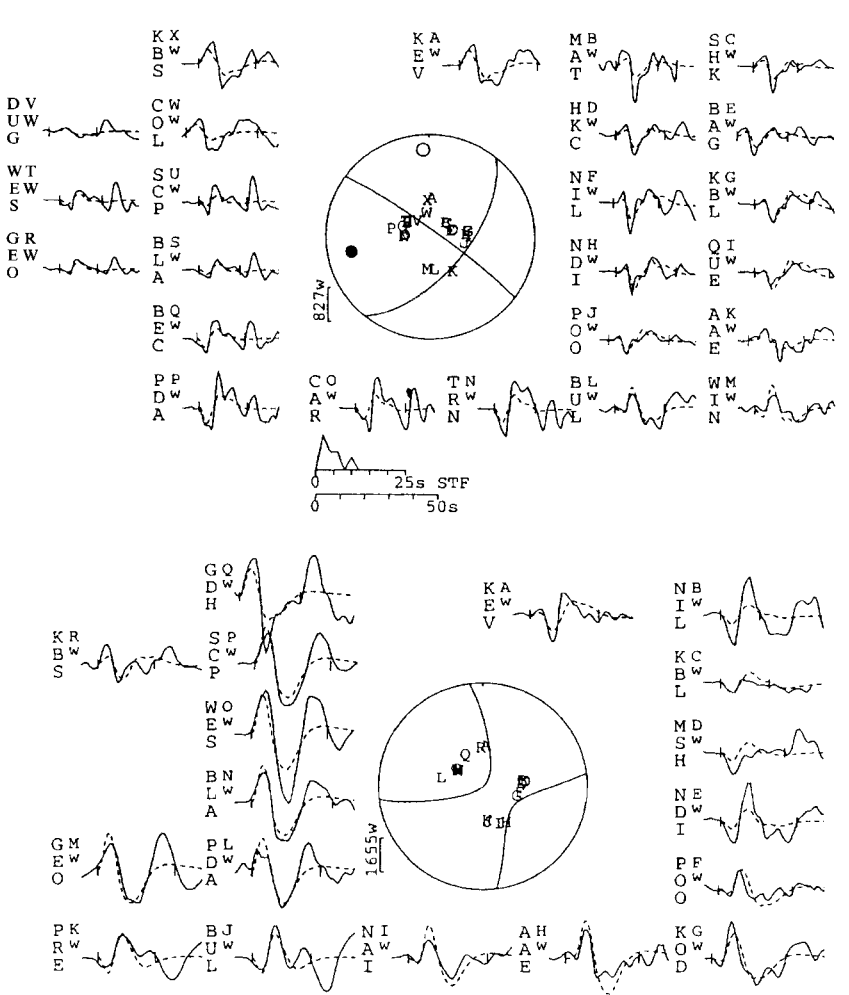

Figure A10. Minimum-misfit solution for the earthquake of 1972 September 17.

Downloaded from http://gji.oxfordjournals.org/ at Observatoire de la CÃ´te d'Azur - Geoazur on December 13, 2016

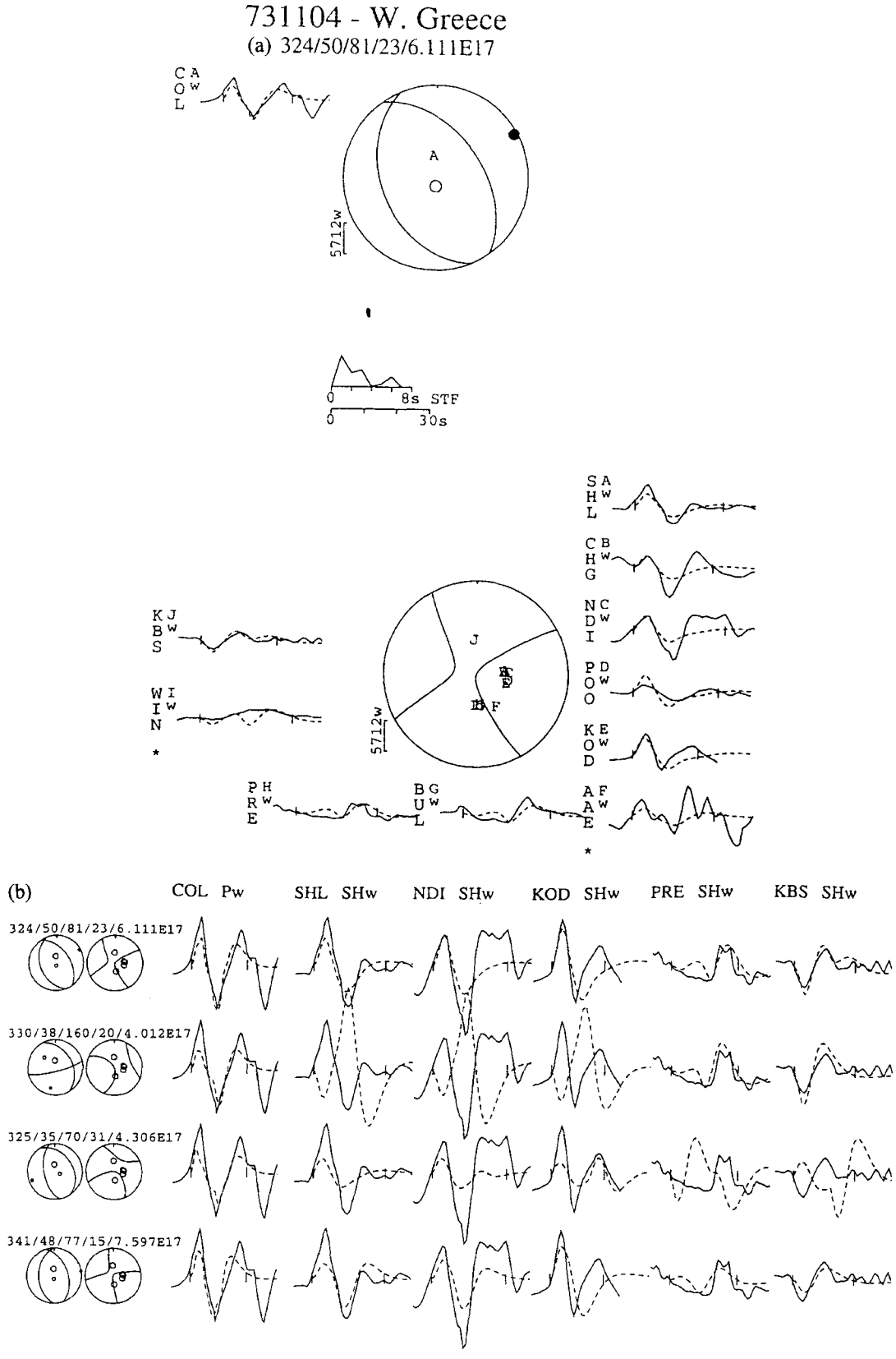

Figure A11. (a) Minimum-misfit solution for the earthquake of 1973 November 4. (b) A comparison of different source mechanisms for the event of 1973 November 4. Line 1 shows the minimum-misfit solution. Line 2 shows one of the two mechanisms proposed by Anderson & Jackson (1987) for this event (the other is close to our minimum-misfit solution). Line 3 shows the mechanism obtained when the dip of the NE-dipping plane is fixed at a shallower value (as seen for events to the north and south) and the other parameters are allowed to vary freely. Line 4 shows the mechanism obtained when the depth is fixed at a shallower value than that obtained in the minimum-misfit solution and the other parameters are allowed to vary freely in the inversion.

Downloaded from http://gji.oxfordjournals.org/ at Observatoire de la CÃ´te d'Azur - Geoazur on December 13, 2016

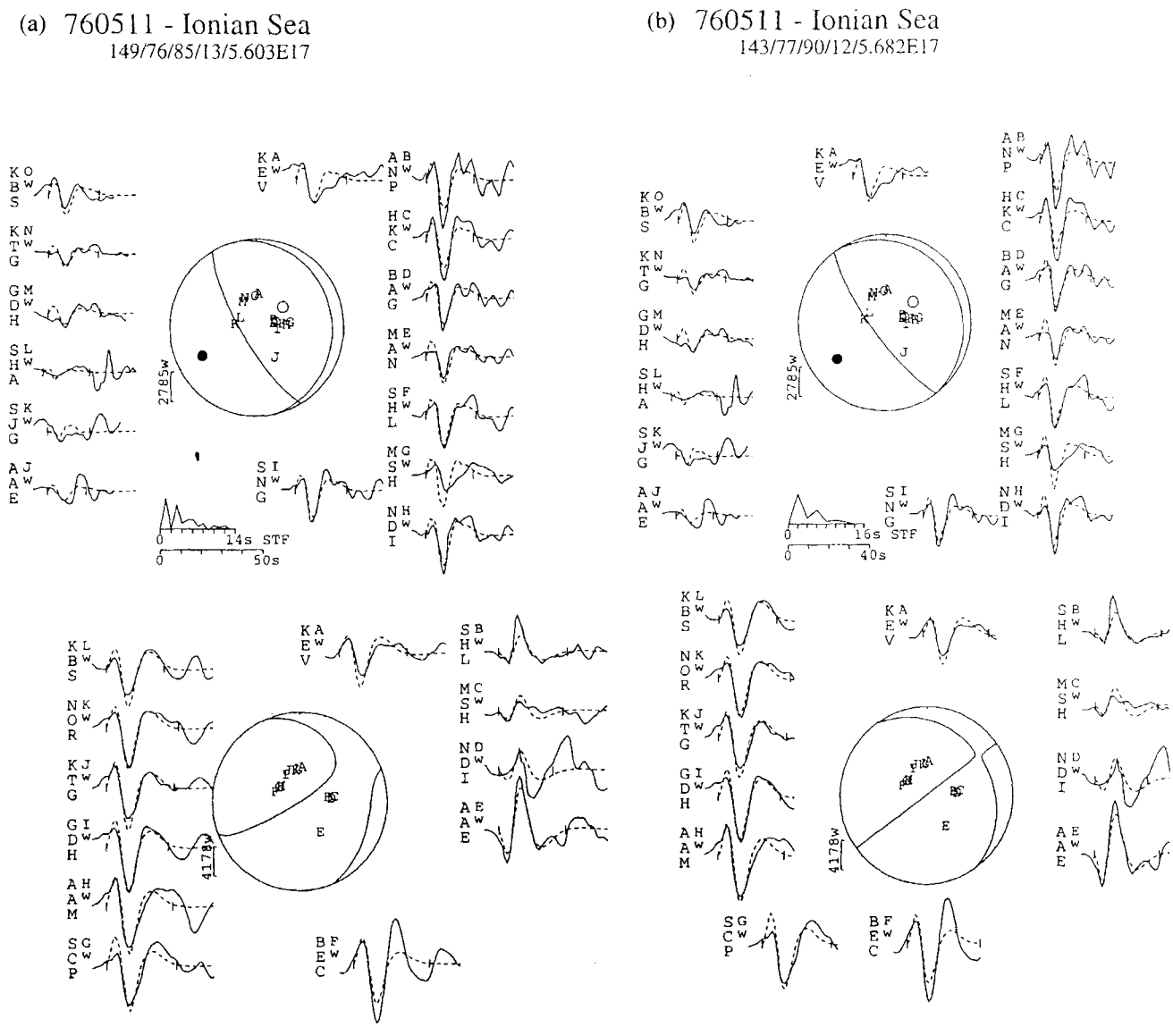

Figure A12. (a) Minimum-misfit solution for the earthquake of 1976 May 11. (b) The preferred solution for the earthquake of 1976 May 11. In this case the rake has been fixed at 90° to give a pure dip-slip thrust mechanism.

Downloaded from http://gji.oxfordjournals.org/ at Observatoire de la CÃ´te d'Azur - Geoazur on December 13, 2016

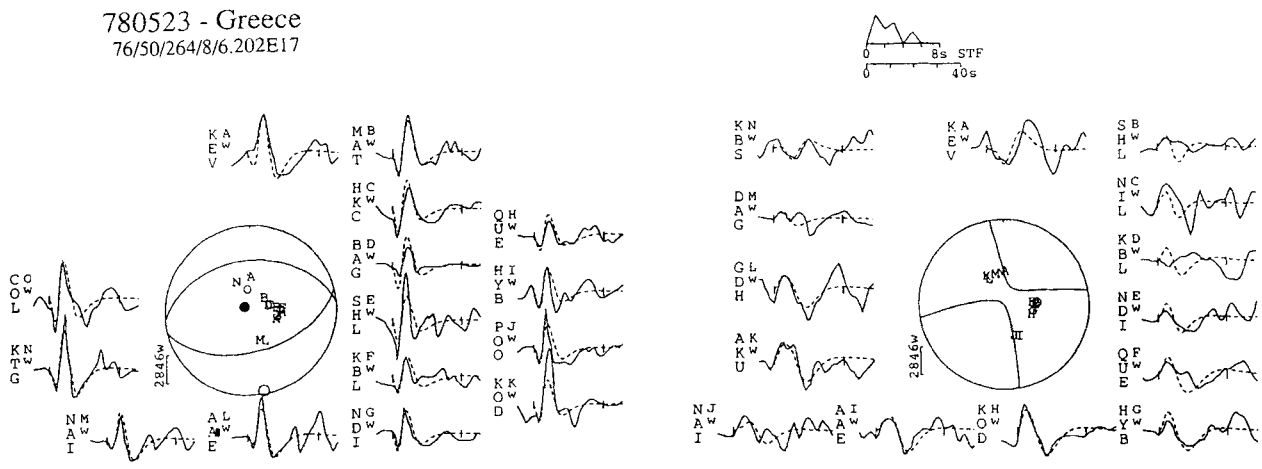

Figure A13. Minimum-misfit solution for the earthquake of 1978 May 23. The left-hand plot shows the *P*-wave radiation and the right-hand plot the *S*-wave radiation.

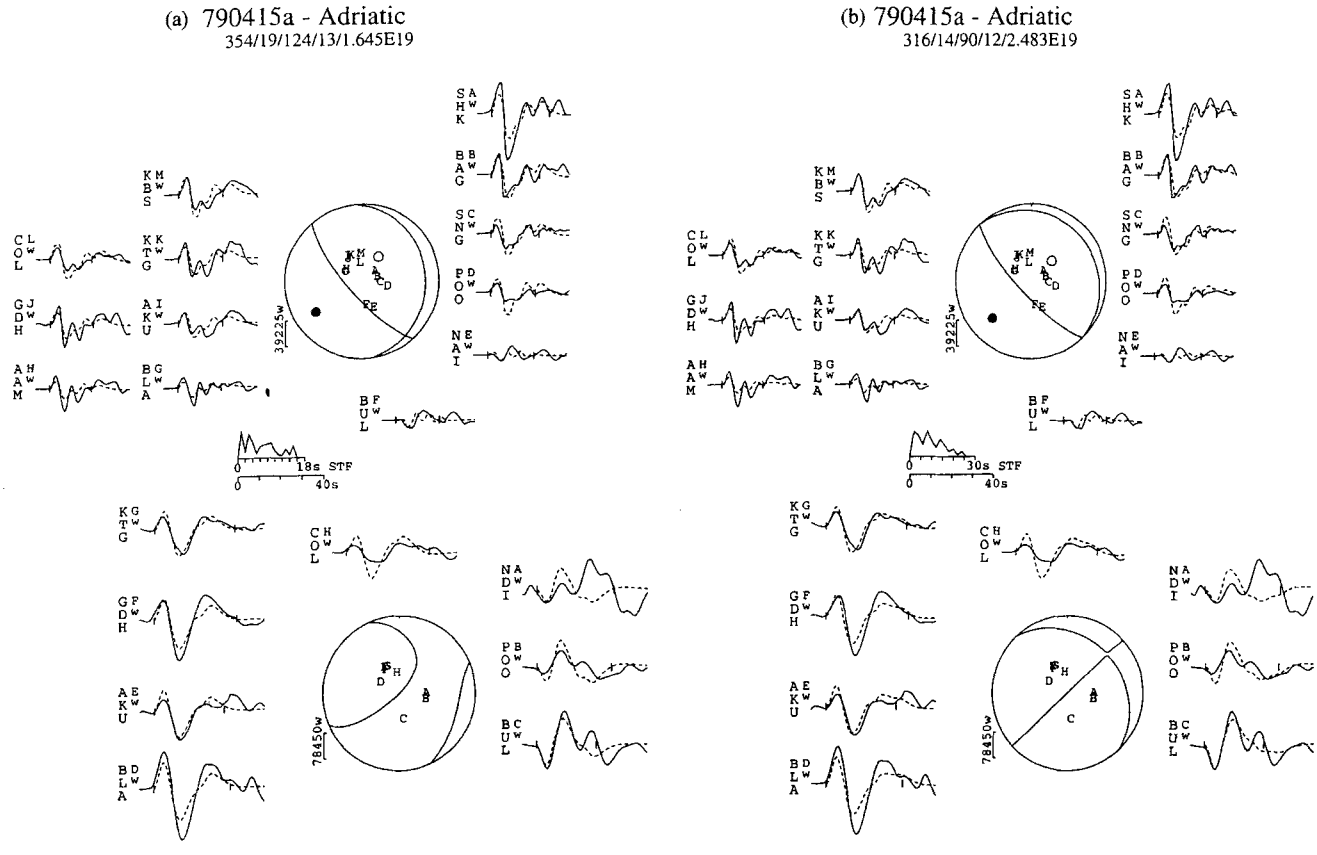

Figure A14. (a) Minimum-misfit solution for the earthquake of 1979 April 15 at 06:19 hr. (b) The preferred solution for the earthquake of 1979 April 15 at 06:19 hr. In this case the rake has been fixed at 90° to give a pure thrust mechanism with the shallow-dipping plane parallel to the bathymetry.

Downloaded from http://gji.oxfordjournals.org/ at Observatoire de la CÃ´te d'Azur - Geoazur on December 13, 2016

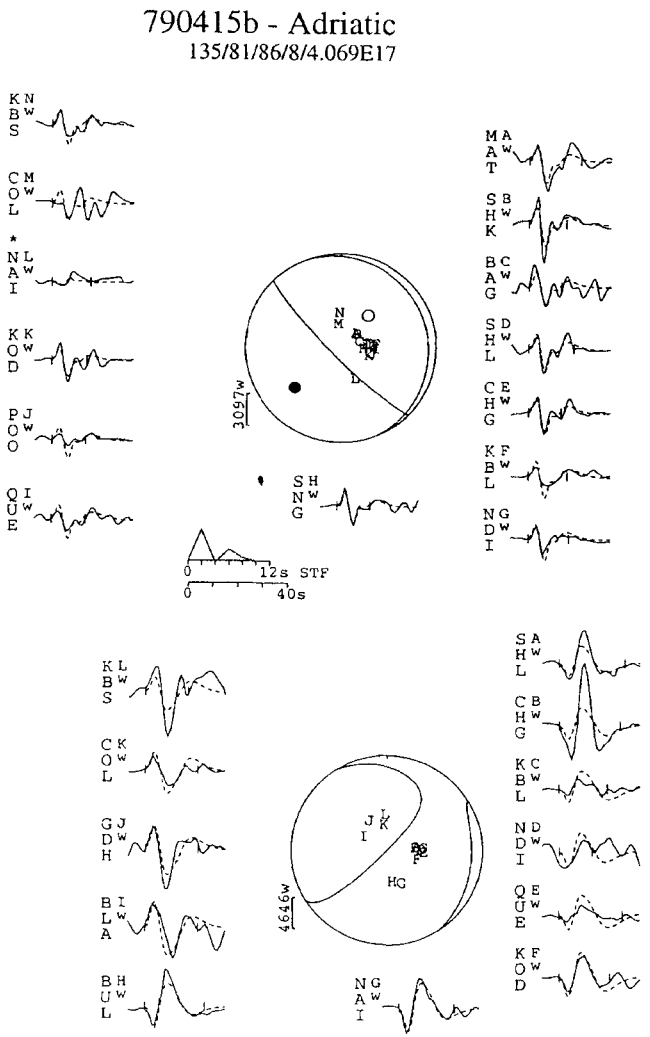

Figure A15. Minimum-misfit solution for the earthquake of 1979 April 15 at 14:43 hr.

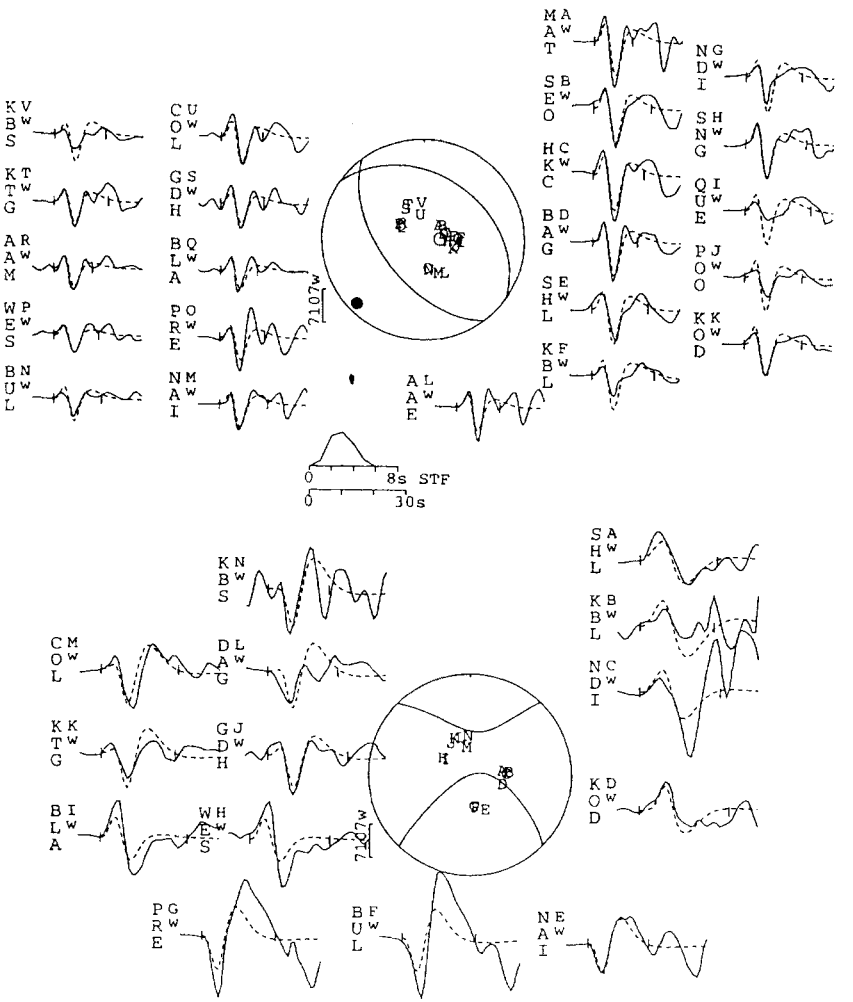

Figure A16. (a) Minimum-misfit solution for the earthquake of 1979 May 24. (b) The preferred solution for the earthquake of 1979 May 24. In this case the rake has been fixed at 90 to give a pure thrust mechanism with the E-dipping plane parallel to the bathymetry. (c) A comparison of different source mechanisms for the event of 1979 May 24. The top line shows the fit at six stations for the preferred solution as shown in Fig. 20 (b). Line 2 shows a mechanism where the dip of the NE-dipping nodal plane has been fixed at a shallower angle similar to the events of 1979 April 15.

Downloaded from http://gji.oxfordjournals.org/ at Observatoire de la CÃ´te d'Azur - Geoazur on December 13, 2016

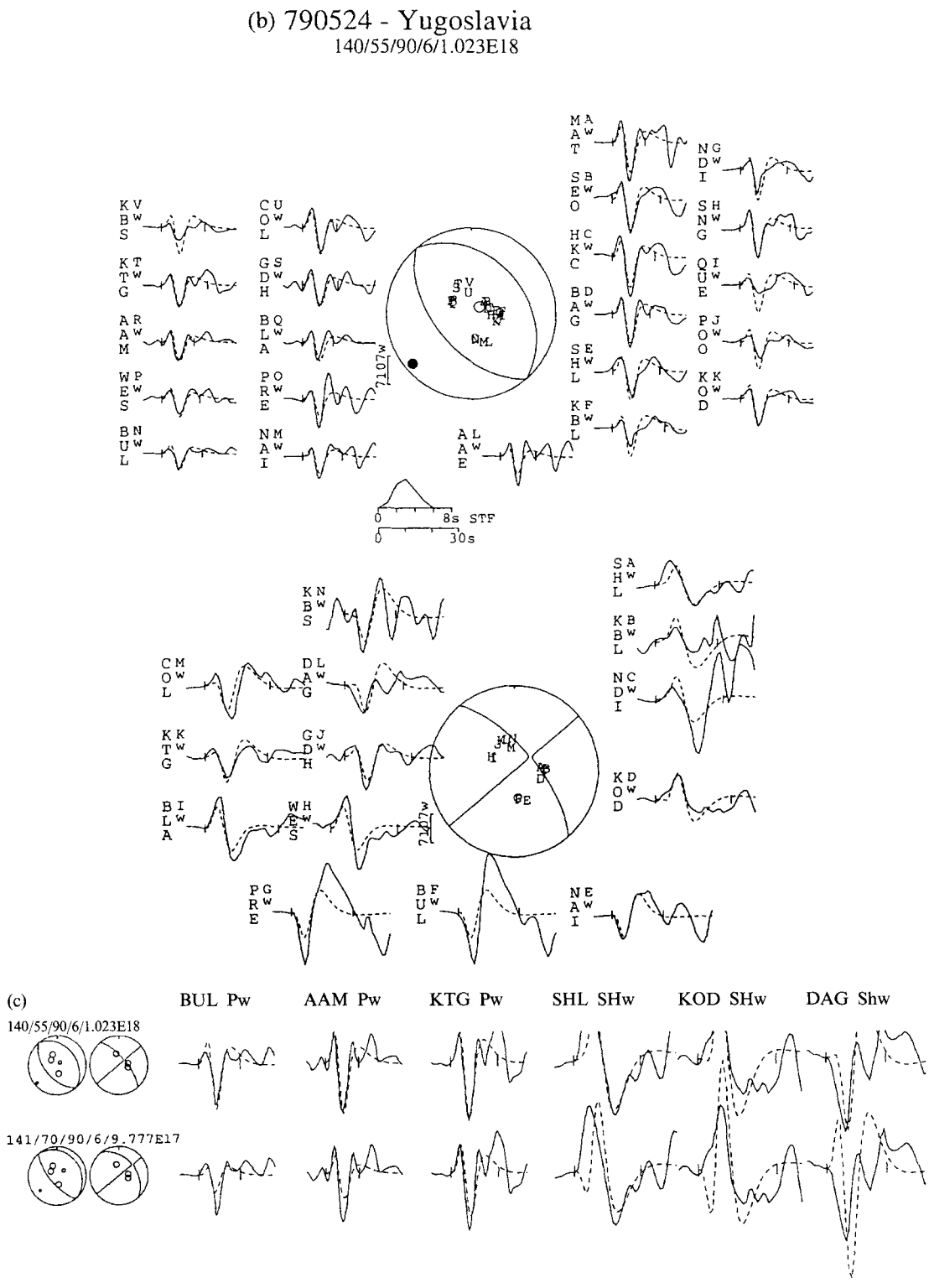

Figure A16. (*Continued.*)

Downloaded from http://gji.oxfordjournals.org/ at Observatoire de la CÃ'te d'Azur - Geoazur on December 13, 2016

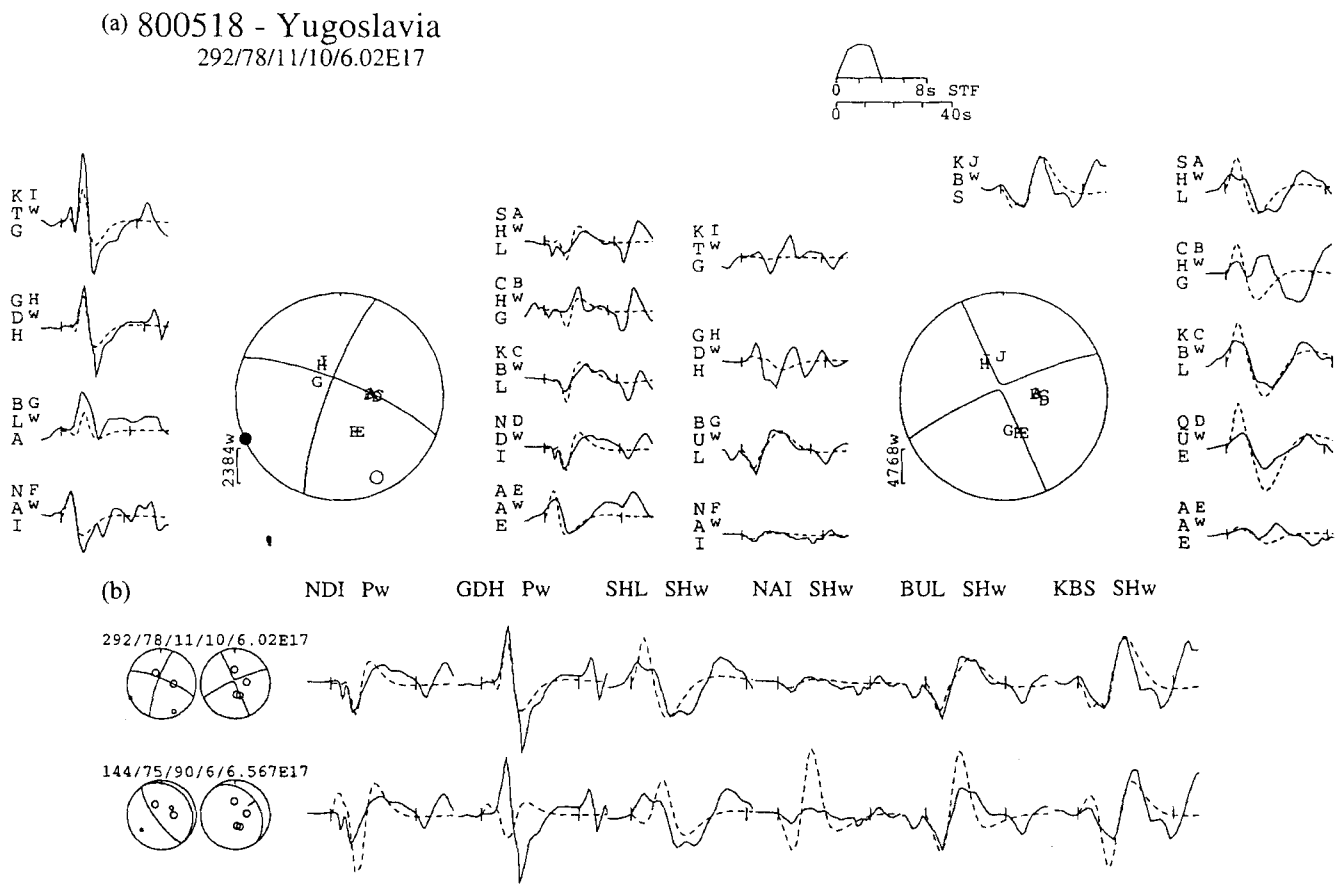

Figure A17. (a) Minimum-misfit solution for the earthquake of 1980 May 18. The left-hand plot shows the *P*-wave radiation and the right-hand plot the *S*-wave radiation. (b) A comparison of two different source mechanisms for the event of 1980 May 18. The top line shows the minimum-misfit solution. Line 2 shows a thrust mechanism of similar orientation to the Montenegran events which was also compatible with first-motion readings (Anderson & Jackson 1987).

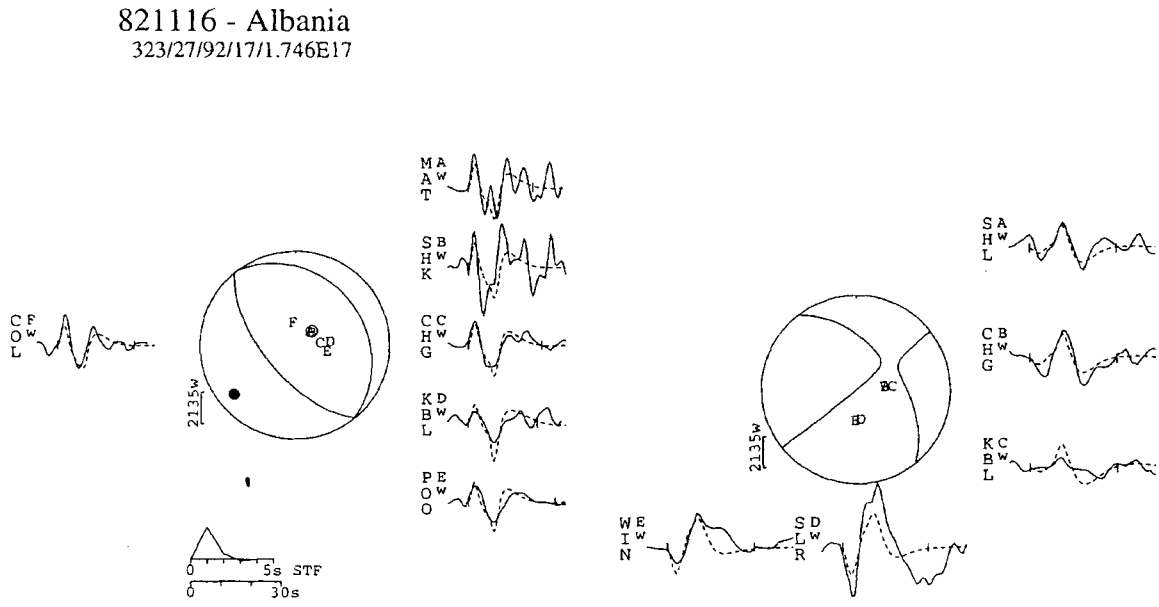

Figure A18. Minimum-misfit solution for the earthquake of 1982 November 16. The left-hand plot shows the *P*-wave radiation and the right-hand plot the *S*-wave radiation.

Downloaded from http://gji.oxfordjournals.org/ at Observatoire de la CÃ'te d'Azur - Geoazur on December 13, 2016

© 1997 RAS, GJI 131, 559–594

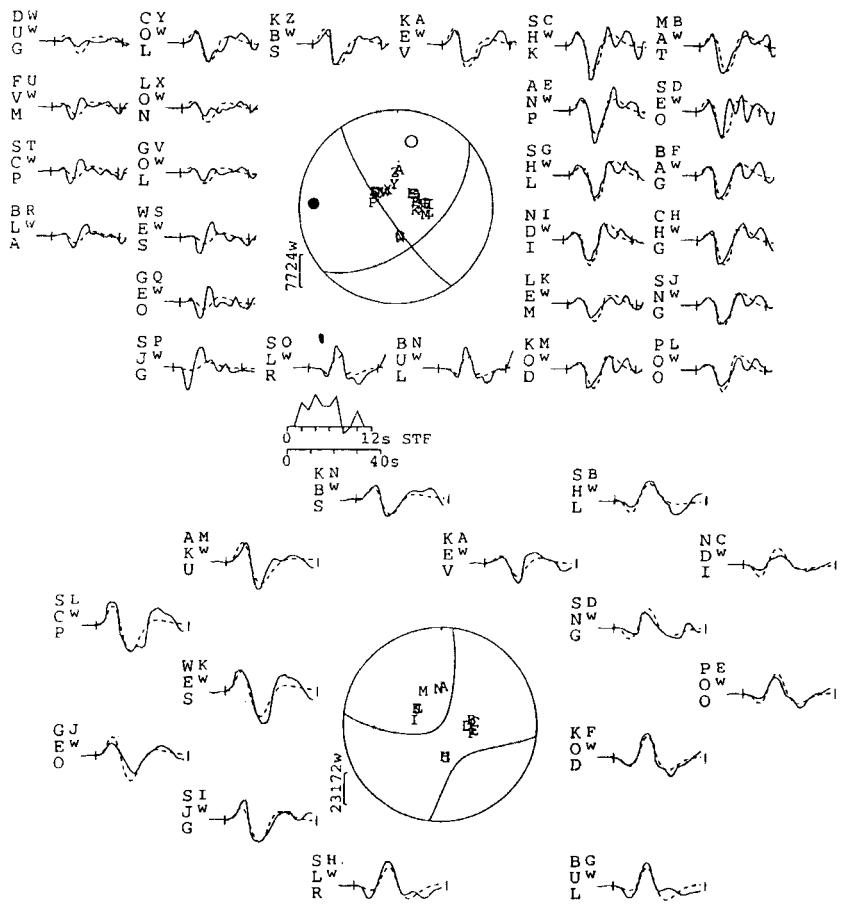

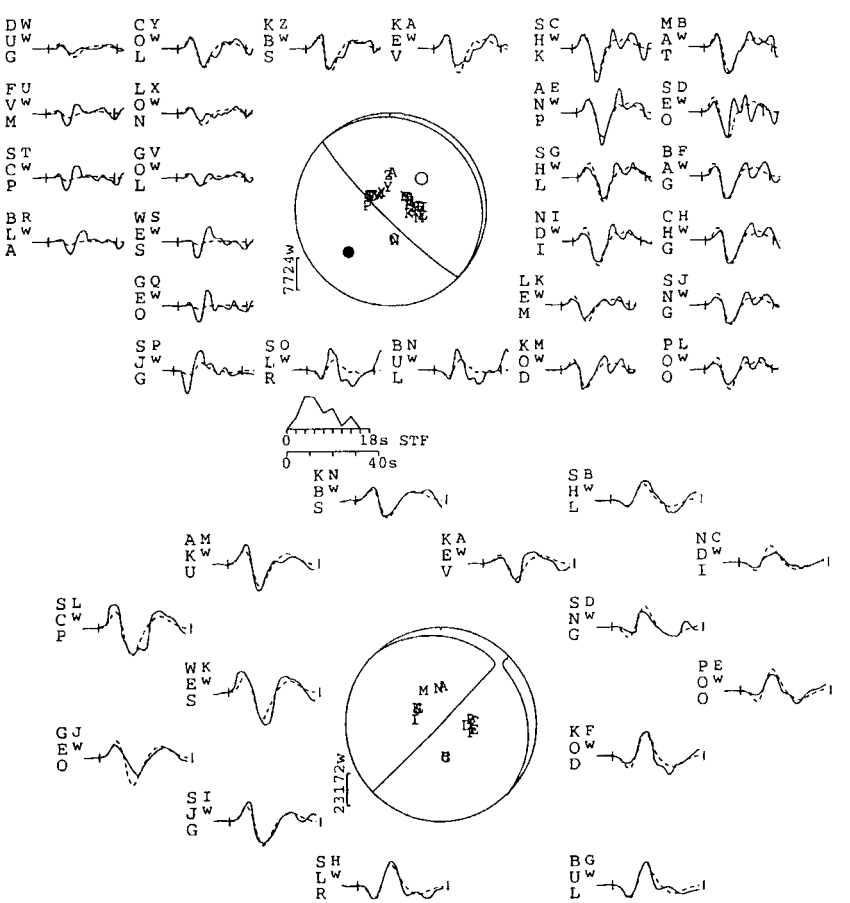

Figure A19. (a) Minimum-misfit solution for the earthquake of 1983 January 17. This solution is preferred to the one shown in Fig. A19 (b), which fits the data equally well, on the basis that it is more compatible with observed bathymetry and the aftershock pattern. (b) A mechanism for the earthquake of 1983 January 17 with a thrust solution. Note that this fits the waveforms equally well at all stations and better for some *SH* phases.

Downloaded from http://gji.oxfordjournals.org/ at Observatoire de la CÃ´te d'Azur - Geoazur on December 13, 2016

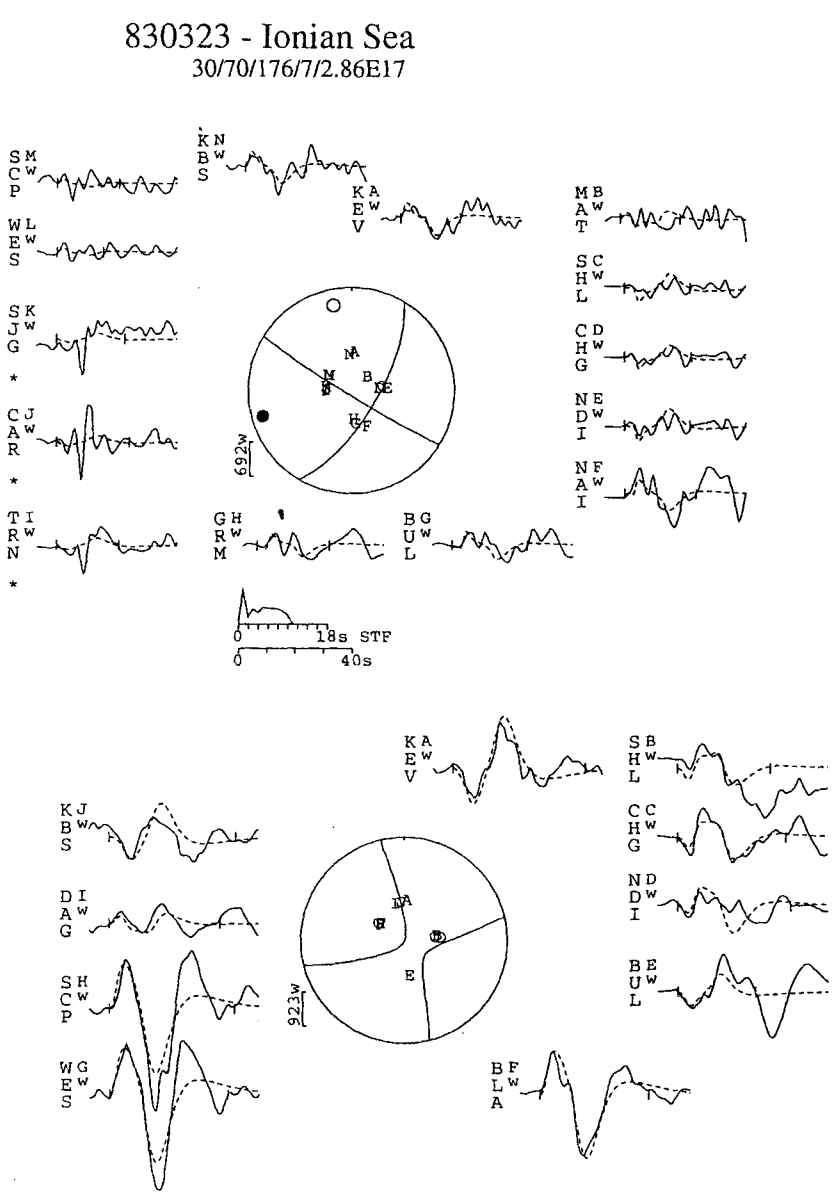

Figure A20. Minimum-misfit solution for the earthquake of 1983 March 23.

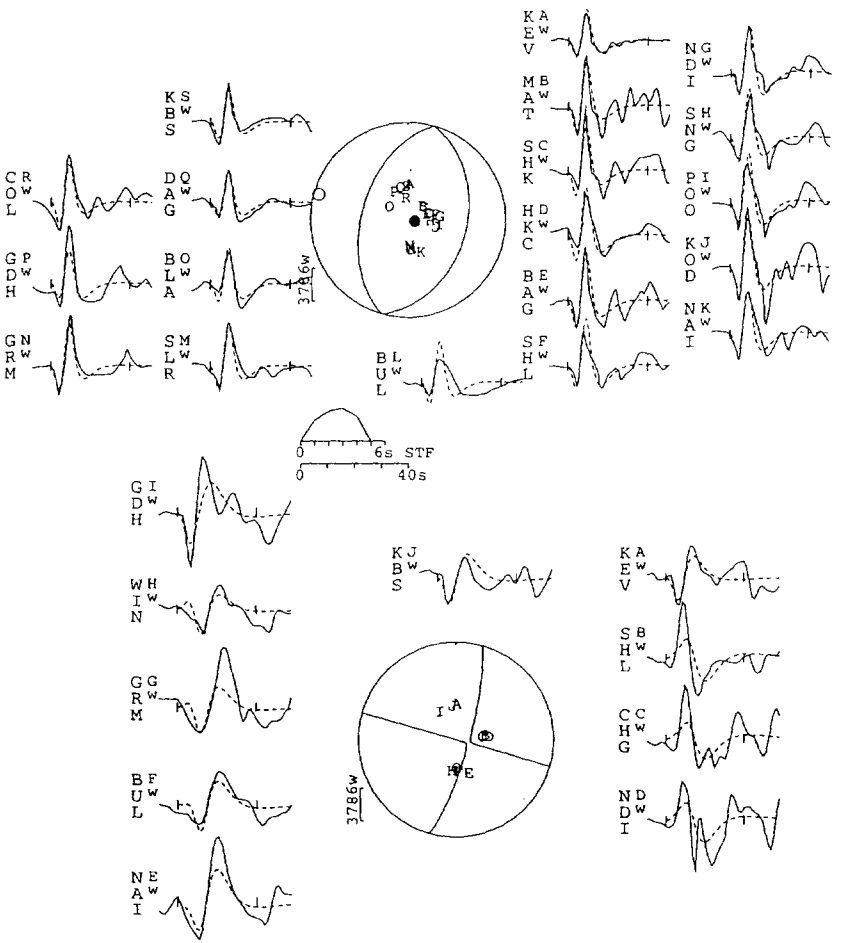

Figure A21. Minimum-misfit solution for the earthquake of 1986 September 13.

Downloaded from http://gji.oxfordjournals.org/ at Observatoire de la CÃ´te d'Azur - Geoazur on December 13, 2016